The Journal of Undergraduate Research in Physics

CONTENTS

VOLUME 10, NUMBER 1

OCTOBER, 1991

Published by the Physics Department of Guilford College
for
The American Institute of Physics and The Society of Physics Students

THE JOURNAL OF UNDERGRADUATE RESEARCH IN PHYSICS

This journal is devoted to research work done by undergraduate students in physics and its related fields. It is to be a vehicle for the exchange of ideas and information by undergraduate students. Information for students wishing to submit manuscripts for possible inclusion in the Journal follows.

ELIGIBILITY

The author(s) must have performed all work reported in the paper as an undergraduate student(s). The subject matter of the paper is open to any area of pure or applied physics or physics related field.

SPONSORSHIP

Each paper must be sponsored by a full-time faculty member of the department in which the research was done. A letter from the sponsor, certifying that the work was done by the author as an undergraduate and that the sponsor is willing to be acknowledged at the end of the paper, must accompany the manuscript if it is to be considered for publication.

SUBMISSION

Two copies of the manuscript, the letter from the sponsor and a telephone number where the author can be reached should be sent to:

Dr. Rexford E. Adelberger, Editor
THE JOURNAL OF UNDERGRADUATE
RESEARCH IN PHYSICS
Physics Department
Guilford College
Greensboro, NC 27410

FORM

The manuscript should be typed, double spaced, on 8 1/2 x 11 inch sheets. Margins of about 1.5 inches should be left on the top, sides, and bottom of each page. Papers should be limited to fifteen pages of text in addition to an abstract (not to exceed 250 words) and appropriate drawings, pictures, and tables. Manuscripts may be submitted on a disk that can be read by a MacIntosh™. The files must be compatible with MacWrite™ or MicroSoft Word™. Illustrations should be in a MacDraw™ or MacPaint™ PICT format.

ILLUSTRATIONS

Line drawings should be made with black ink on plain white paper. Each figure or table must be on a separate sheet. Photographs must have a high gloss finish.

CAPTIONS

A brief caption should be provided for each illustration or table, but it should not be part of the figure. The captions should be listed together at the end of the manuscript

EQUATIONS

Equations should appear on separate lines, and may be written in black ink.

FOOTNOTES

Footnotes should be typed, double spaced and grouped together in sequence at the end of the manuscript.

PREPARING A MANUSCRIPT

A more detailed set of instructions for authors wishing to prepare manuscripts for publication in the Journal of Undergraduate Research in Physics can be found in Volume 8 #1 which appeared in October of 1989.

SUBSCRIPTION INFORMATION

The Journal is published bianually, with issue # 1 appearing in October and issue # 2 in April of the next year. There are two issues per volume.

TYPE OF SUBSCRIBER	PRICE PER VOLUME
Individual	$US 5.00
Institution	$US 10.00

Foreign subscribers add $US 2.00 for surface postage, $US 10.00 for air freight.

Back issues may be purchased by sending $US 15.00 per volume to the editorial office.

To receive a subscription, send your name, address, and check made out to **The Journal of Undergraduate Research in Physics (JURP)** to the editorial office:

JURP
Physics Department
Guilford College
Greensboro, NC 27410

The Journal of Undergraduate Research in Physics is the sent to each member of the Society of Physics Students as part of their annual dues.

VOLUME 10 1991-92

The Journal of Undergraduate Research in Physics

Published by the Physics Department
of Guilford College
for

The American Insitute of Physics
and
The Society of Physics Students

ISSN 0731 - 3764

WE'VE COME A LONG WAY - TEN YEARS OF JURP

Rexford E. Adelberger - Editor

Some fifteen years ago, a few physics teachers who were convinced that getting undergraduates involved in research was the best way to get students interested in learning to be professional physicists, talked together at the regional and national meetings of the Society of Physics Students about the need for a journal that was dedicated to publishing the work done by such individuals. The research projects that most undergraduate students can successfully complete during their brief stay at college seldom met the rigorous requirements of the archival journals of the American Institute of Physics. This does not mean that the work lacked new physics and clever insights, it was just not of the scope expected of people whose profession is to do research in physics. Yet, we were convinced that the learning and rewards that come from writing up the research in a professional manner and learning to communicate using the professional media had a definite place in the undergraduate program of study in physics.

Eleven years ago, this group, headed by Professor Ray Askew, convinced the Council of the Society of Physics Students to support this idea and to try to establish of Journal sponsored by the Society and Sigma Pi Sigma. The Executive Board of the Society approached the American Institute of Physics to financially back the volume of the Journal. When the AIP agreed in principle to this request, the Society of Physics Students got one of the group to agree to be the editor/publisher, purchased an Apple II+ computer with a daisy wheel printer to set the type and sent out a call for papers. As a model for the Journal, we used the successful *Journal of Undergraduate Mathematics*, published by J.R. Boyd at Guilford College. For the next 9 years, the Journal of Undergraduate Research in Physics has appeared twice during the academic year.

Three years ago, the Society of Physics Students decided to include the Journal as part of the membership benefits of the Society. This increase in readers to over 6,000 per issue had a big effect on the number and quality of manuscripts received for publication. At the same time, the AIP once again provided financial support to upgrade the computer facilities of the editorial office to a MacIntosh SE and a laser printer. This not only allowed us to produce a more professional looking copy, but cut down significantly on the time required to put together an issue.

When an manuscript arrives at the editorial office at Guilford College, it is read by the editor. If the material does not meet the publishing requirements of the Journal, a letter to that effect is sent to the author. The faculty sponsor of the paper provides the evaluation of the physics and that the work was done by the undergraduate student submitting the manuscript.

Those manuscripts that seem to be appropriate for the Journal are then then undergo another editorial review. This reviewer (often an advanced undergraduate student) makes an evaluation of the presentation of the work. At this point, there are three possible paths that the manuscript can take. If the reviewer finds it interesting and understandable, the editor enters the manuscript into the computer to produce a proof copy which is sent to the author and to the sponsor for correction. If the reviewer finds the manuscript interesting, but in need of major rewriting - usually to include more background and explanation of what is going on - a letter reflecting these comments with many suggestions as to how to rewrite the manuscript is sent to the author . If the reviewer feels that this paper is not research, but is something that is either a piece of work that would be done in a normal lab, or that the work is so complicated that they can not understand what it is about, the paper is sent to a member of the Editorial Review Board for refereeing. The comments of this referee are then sent to both the author and the sponsor of the paper.

There are also the subscriptions that must be looked after. About 250 libraries and about 50 individuals subscribe to the Journal. There are some 600 physics departments in the USA, so please check to see if your library gets the Journal. It will be the cheapest and most read journal in their collection.

As you can see, this is a worth while, but rather labor intensive operation. It takes the editor just over 100 hours to produce a typical issue.

GROUND BASED MEASUREMENTS OF $0_2(^1\Delta g)$ AT 1.58μ *

Douglas Drob **
Embry-Riddle Aeronautical University
Daytona Beach, FL

ABSTRACT

To develop a method for verifying ozone density profiles using a ground based Michelson interferometer, a preliminary study of the twilight airglow (0,1) band of $O_2(^1\Delta g)$ was conducted in the summer of 1990. The data were compared to a theoretical model which involved the dissociation of ozone in the Hartley continuum. The model appears to agree with the data and could provide an insight into ozone density profiles.

INTRODUCTION

Measurements of $O_2(^1\Delta g)$ twilight airglow have been made for at least 30 years. Figure 1 is an illustration of the twilight airglow observation process. Incoming sunlight strikes ozone in the middle atmosphere, resulting in the following process:

$$h\nu(200\text{-}300\text{ nm}) + O_3 \rightarrow O_2(^1\Delta g) + O(^1D).$$

The excited oxygen molecules then make the following transition:

$$O_2(^1\Delta g) \rightarrow O_2(^3\Sigma g) + h\nu(1580\text{ nm}).$$

This near-infrared light, along with scattered sunlight is seen after th sun is well below the horizon.Emissions from the (0,1) band at 1.58μ were first discovered in 1958 [1]. The same group made an effort to find the emissions from the (0,0) band at 1.27 μ. This emission was found in 1962 on an airborne experiment. [2] The (0,0) signal appeared much weaker on the ground because of self absorption in the lower atmosphere.

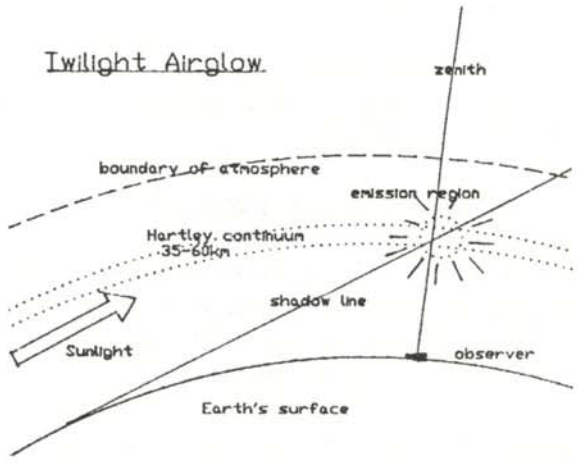

Figure 1
An illustration of the twilight airglow process. Incoming sunlight strikes ozone in the middle atmosphere, resulting in the following process:
$h\nu$ (200 nm-300 nm) + $O_3 \rightarrow O_2(^1\Delta g) + O(^1D)$.
The excited oxygen molecules then make the following transition:
$O_2(^1\Delta g) \rightarrow O_2(^3\Sigma g) + h\nu(1580\text{ nm})$.
This near-infrared light, along with scattered sunlight is seen after th sun is well below the horizon.

The mechanism for the formation of $O_2(^1\Delta g)$ in the upper stratosphere and lower mesosphere was attributed to ozone dissociation in the Har-

---

Douglas Drob graduated in April 1991 with a B. Sc. in Engineering Physics from Embry-Riddle Aeronautical University. He has been admitted to the Atmospheric, Oceanic and Space Sciences graduate program at the University of Michigan.

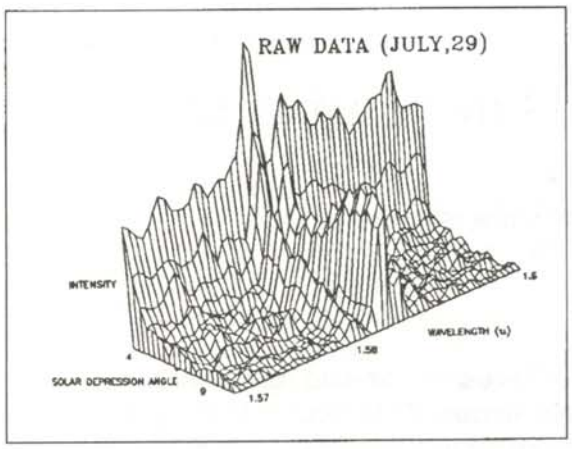

Figure 2
A series of twilight spectra between 1.57μ and 1.60μ taken 1.57 minutes apart with a Michelson Interferometer. The $O_2(^1\Delta g)$ emission occurs at 1.58μ near the 1.583μ OH emission

tley continuum.[3] The validity of this statement was checked using ground based measurements of the (0,0) emission.

The observations showed a seasonal change in the brightness of the emissions, but were unexplained. Later, [4] it was shown that these changes are linked to seasonal changes in ozone density profiles. Ten years of aircraft data on the (0,0) band were used in this study.

A ground based study of the (0,1) band was conducted in June and July of 1990 at the University of Michigan, Ann Arbor. We wished to determine if the observed $O_2(^1\Delta g)$ twilight emissions successfully be obtained with a Michelson interferometer. The ultimate goal of our study is to investigate the possibility of developing a method of verifying ozone density profiles using ground based $O_2(^1\Delta g)$ data and an appropriate model.

OBSERVATIONS

The system used in data acquisition was a commercially available Michelson interferometer [5] with an InGaAr detector with a signal to noise ratio of about 30 and a 4 cm^{-1} resolution. Though the system was designed for absorption spectroscopy, it was modified by its producer for emission spectroscopy. The manufacturer also privided software that was menu driven and could be configured for automated data acquisition.

Scans from 2μ to 8μ, looking in the zenith, were taken beginning 15 minutes before sunset. The scan time was set at 1.58 minutes, which corresponds to about 0° 24' 30"of solar arc. Figure 2 shows how the spectrum from 1.57μ to 1.6μ changes as a function of the solar depression angle.

DATA REDUCTION

Data reduction began by examining all the spectra to find where the $O_2(^1\Delta g)$ emissions first appeared on the solar background. The region from 1.57μ to 1.60μ was then abstracted from the data until the $O_2(^1\Delta g)$ emissions diminished to noise levels. The solar background to be subtracted was calculated by excluding the $O_2(^1\Delta g)$ and OH lines at 1.58μ at 1.583μ respectively, while smoothing and averaging the data.

Figure 3 shows examples of the abstracted regions, results of smoothing and the solar background average. The average was then subtracted from the single $O_2(^1\Delta g)$ peak point at 1.58μ unless it was negative. The final step was to convert scan times to corresponding solar depression angles using an ephemeris program on a computer.

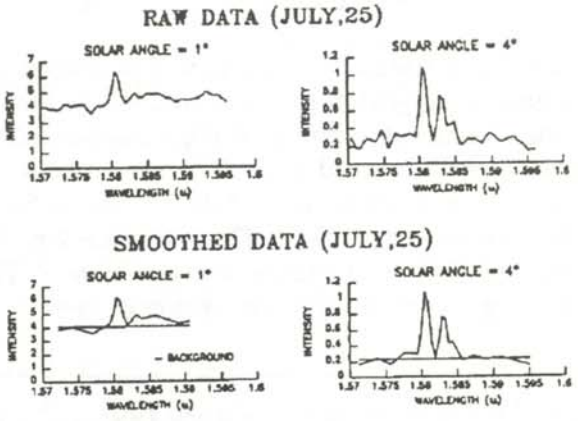

Figure 3
An illustration of the raw data and the procedure used to determine the $O_2(^1\Delta g)$ brightness above that of the decaying solar background.

The theoretical Vallance Jones-Gattinger model used for comparison was generated by graphically interpolating data on the seasonal variation of the twilight airglow band [6]. The model provided 1.58μ $O_2(^1\Delta g)$ data based on 8 possible chemical reactions covering solar depression angles from 10 to -10 degrees. More complex models are known [7], but were not used in this analysis. Rate equations were created assuming no vertical transport, setting production equal to loss and providing the corresponding rate constants, some of which were functions of temperature and solar depression angle. These equations were solved numerically using daytime equilibrium concentrations of O and O_2. Finally, the $O_2(^1\Delta g)$ emissions were integrated over their optical path to the ground, giving observed brightness as a function of time.

RESULTS

To make a good comparison, the experimental data were normalized to the theoretical model. This eliminated the need to covert the experimental data from a relative intensity scale to an absolute intensity scale. The results, shown in Figure 4, show a fair correlation between the model and the experimental data.

There are possible indications of a seasonal variation. The Vallance Jones-Gattinger model uses midwinter parameters, while the data are representative of mid summer. The observations show a slightly lower rate of decay, possibly indicating the changes in ozone density profiles and other factors. However, at this point in the study, it is too early to rule out an error in modeling or data reduction.

The data also suggest a new question: What is the cause of the small oscillations in the experimental data? Could it be that there are winds bringing clouds of $O_2(^1\Delta g)$ into a depleted region above the instrument, or is it due to gravitational effects? These questions may merit further investigation.

These results show that excellent $O_2(^1\Delta g)$ data can be obtained with a Michelson interferometer. To make better use of the data, a new model should be generated using new rate constants

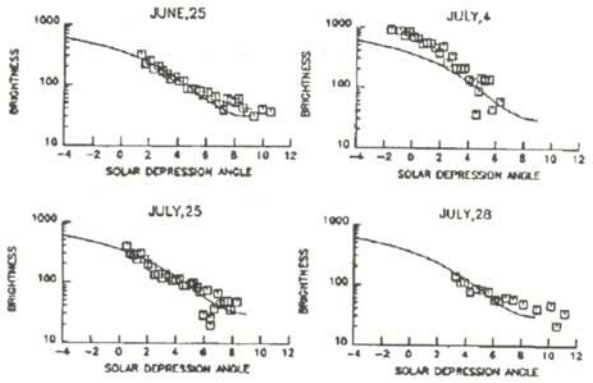

Figure 4
A comparison of the observed decay of $O_2(^1\Delta g)$ [the square data points] looking in the zenith and a theoretical model [the line] involving prodiction of $O_2(^1\Delta g)$ by dissociation of ozone in the Hartley continuum.

and daytime equilibrium concentrations corresponding to the date of the observations and geographical location of the observing site. A further calculation of actual intensity of the observational data would allow for measurement of seasonal variations in absolute intensity.

ACKNOWLEDGEMENTS

The author would like to thank Dr. Rick Nicjewski for giving the the information, equipment and guidance that was necessary to do this experiment. He would also like to thank Dr. Tim Killeen and those in charge of the Research Experience for Undergraduates Program for the opportunity to do this work at the University of Michigan Space Physics Research Lab.

REFERENCES

* This work was done when the author was a participant in the Research Experience for Undergraduates Program at the University of Michigan Space Physics Research Lab, Ann Arbor, MI 48109.

1. A. Vallance Jones and A.W. Harrison," $^1\Delta g$ - $^3\Sigma g$ O_2 Infrared Emission Band in the Twilight Air Glow Spectrum", J. Atmos. Terr. Phys, 13, 1958, p. 45.
2. J.F. Noxon and A. Vallance Jones, "Observation of the (0,0) band of the (^1Dg - $^3\Sigma g$) system of O_2 in the Day and Twilight Airglow" , Nature, 196, 1962, p. 157.
3. A. Vallance Jones and R.L Gatinger, 'The Seasonal Variation and Excitation Mechanism of the 1.58μm ($^1\Delta g$ - $^3\Sigma g$) Twilight Airglow Band", Planet. Space Sci., 11, 1963, p. 961.

4. J.F. Noxon, "A Global Study of O_2 ($^1\Delta g$) airglow: Day and Twilight", Planet. Space Sci. 30, 1981, p. 545.
5. Bomen, Inc. Model # MB140.
6. A Vallance Jones and R.L Gattinger, op.cit.
7. R.L. Gattinger, "Observation and Interpretation of the $^1\Delta g$ - $^3\Sigma g$ O_2 Airglow Emissions", Can. J. Phys. 46, 1968, p. 1613.

FACULTY SPONSOR

Dr Rick Nicjeweski
Space Physics Research Laboratory
2455 Hayward
Ann Arbor, MI 48190

THE STUDY OF A HYPOTHESIZED STRUCTURAL ZONE USING THE GRAVITY METHOD OF GEOPHYSICAL EXPLORATION

Christopher Meinen and Paul Ferlemann
Physics Department
Luther College
Decorah, IA 52101

ABSTRACT

A gravity survey was conducted over approximately 2600 square km of northeast Iowa. This survey was undertaken to provide detailed gravity coverage and to investigate the sources of gravity anomalies in the study area. Two additional objectives were to use gravity data to test for the presence of the Fayette Structural Zone previously identified on the basis of linear magnetic anomalies and to look for an extension of this zone beyond the limits defined by the magnetic anomalies. A total of 427 gravity stations were occupied and combined with existing data from the Geological Survey Bureau of Iowa to produce the gravity interpretation. A Bouguer gravity anomaly map was prepared and profile analysis undertaken to examine the source configuration of intrusive bodies located within the basement of the study area. The gravity data, when combined with available magnetic and drill hole information, indicate a predominantly granitic basement with mafic and/or ultramafic intrusive bodies and a small clastic basin. Interpretation of the gravity data, based on modeling studies, failed to confirm the existence of a fault or fault zone at the presumed location of the Fayette Structural Zone. The gravity data also failed to indicate a northeastern extension of the Fayette Structural Zone beyond the location mapped previously by magnetic methods.

INTRODUCTION

A short glossary of terms has been provided at the end of the paper to help the reader with some geologic and geophysical terms. These terms are pesented roughly in the order of their appearance in the text.

This study used the gravity method to investigate basement geology in the vicinity of the hypothesized Fayette Structural Zone in northeast Iowa (Figure 1). This feature has been identified on the basis of a linear magnetic anomaly which strikes roughly from the northeast corner of Black Hawk County to the east central portion of Fayette County. Although detailed magnetic data are available for this area, existing gravity data were based on observations made at approximately 6 mile intervals. This spacing is insufficient to adequately define local effects due to faulting. In our survey, gravity observations at approximately 1 mile intervals were made.

In 1966, an airborne magnetic survey was flown for the Iowa Geological Survey by the Aero Service Corporation. The results [1] indicated that a complex magnetic anomaly pattern existed in the eastern portion of Iowa, from roughly 43.25 degrees north latitude to the Minesota border. The study area is dominated by a large magnetic anomaly (the Randalia anomaly) roughly 16 km in diameter with an amplitude of 3.3×10^{-6} T.

Paul graduated from Luther College in 1991. He is pursuing a Ph.D. in aeronautical engineering at the Joint Institute for Advancement of Flight Sciences in Hampton, VA. Chris will be a senior at Luther College where he is finishing his physics and mathematics majors. After he graduates, he plans to go to graduate school in applied physics.

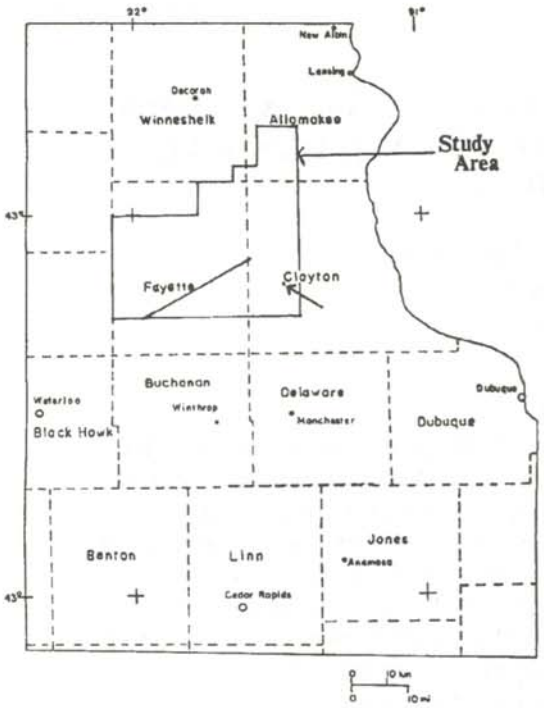

Figure 1
County map of Iowa showing the study area. The arrow indicates the location of the Osborne well. The diagonal line indicates the hypothesized Fayette Structural Zone

This roughly circular anomaly is shown in the western portion of the aeromagnetic anomaly map of the study area, Figure 2. The lineation of the contours along the southern margin of the anomaly is suggestive of basement faulting. [2]

Several other studies have been done in this area: a gravity study of a linear magnetic anomaly located in the extreme southeast portion of our study area [3] ; a detailed gravity study of the Randalia magnetic anomaly [4] and a ground magnetic survey of this same area [5] . The location of the second study coincides with the western portion of the current study area and the data incorporated into this study. The interpretations of these three surveys were taken into consideration during this study.

GEOLOGY

The bedrock in this study area is covered with a veneer of glacial drift ranging in thickness from 0 - 75 m. The topography is level to gently rolling with a local relief of up to 90 m in the eastern portion of the study area. The Paleozoic section varies from 550 to 775 m thick and is composed of Cambrian to Devonian carbonate and clastic sedimentary rocks. Post Paleozoic rocks are absent in northeast Iowa.

Of the few drill holes that penetrate into the basement rocks in northeast Iowa, only one (the Osborne well) is within the survey area.[6] The location of the well is shown in Figure 1. This well penetrated 221 m of ultramafic olivine cumulate immediately beneath the basement surface. A single drill hole in Winneshiek County encountered an olivine gabbro. [7] Ten other basement drill holes occur within the general region of Iowa shown in Figure 1. These wells encountered granite. The wells and the magnetic data suggest a predominantly granitic basement complex locally penetrated by mafic intrusives. An analysis of other available basement well data throughout the state suggests a predominantly grantic basement in Iowa and throughout the upper Midwest.[8]

Gravity and magnetic anomaly maps indicate a complex pattern of Precambrian structure and lithologic variations throughout the Midwest.

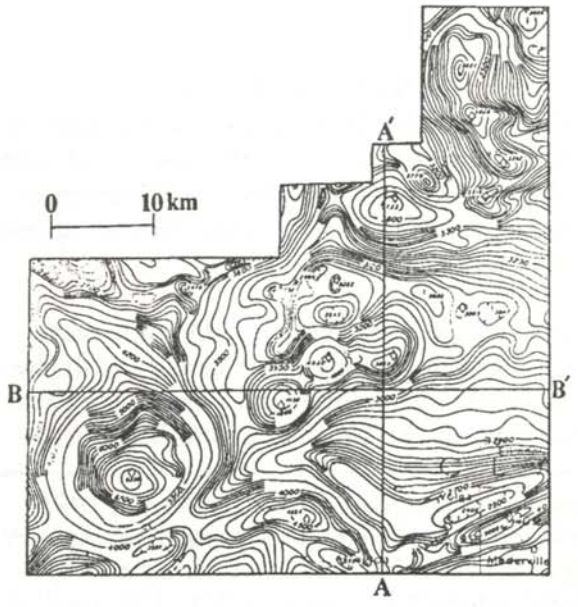

Figure 2
Aeromagnetic map of the study area (taken from reference 1). Contour intervals are 100 nanoTesla

These maps are especially useful because the basement is covered with younger sediments in this area. Basement lithologic variations are typically associated with density and magnetic susceptibility changes. It can be shown that gravity and magnetic anomalies originating from intra-basement lithologic variations are an order of magnitude greater than anomalies originating from within the overlying sedimentary cover. [9]

When interpreting gravity and magnetic maps where the subsurface structure is unknown, the configuration and lithology of the causative bodies are determined from profiles and drill hale data. However, the interpretation of gravity and magnetic maps and profiles is inherently ambiguous. This is true because the physical property contrast is often unknown and little is known about the shape and configuration of the causative bodies. Never-the-less, by combining geological, geophysical and drill hole information, one can arrive at a geologically reasonable interpretation. In northeast Iowa, most geologists have attributed positive gravity and magnetic anomalies to Keweenawan age (1.2 billion year old) mafic intrusives and extrusives.

DESCRIPTION OF RESEARCH

A total of 427 gravity stations with an approximate spacing of 1 mile were occupied in the study area during the summers of 1988 and 1990. All observations were made with a Worden gravity meter. Gravity stations were noted on 7.5 minute topographic maps. The choice of station locations was limited to sites with known elevations as shown on the 7.5 minute topographic maps. Elevations obtained from these maps are accurate to within 2 feet. Nine base stations were established at intervals of approximately one per 7.5 minute map. Loop traverses generally consisted of 5 to 8 station occupations and were closed on base stations in intervals of about 2 hours. This was necessary because the meter readings undergo small variations due to temperature and tidal variations that are not related to gravity variations.

Data reduction was done using standard techniques on a personal computer. A density of 2.67 g/cm^3 was used for the elevation correction. The 1930 International Gravity Formula [10] was used to calculate the theoretical gravity. Bouguer gravity values were obtained by subtracting the theoretical gravity from the observed gravity. The Bouguer gravity values [11] were then entered into a contour program to produce the Bouguer gravity anomaly map of the study area shown in Figure 3.

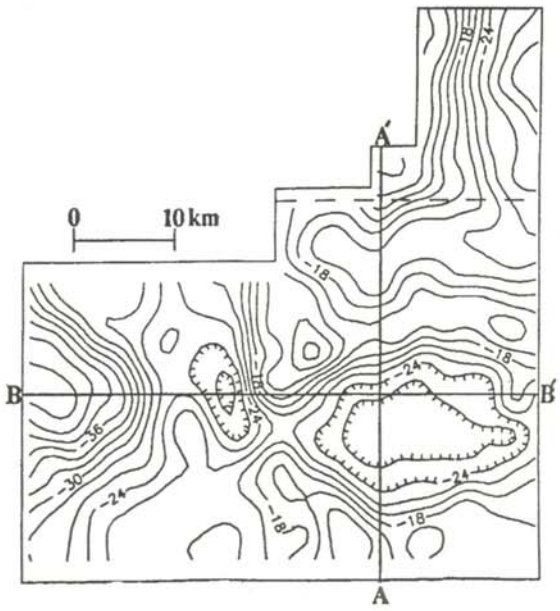

Figure 3
Bouguer gravity anomaly map of the study area. Contour intervals are 2 milligals.

DISCUSSION OF RESULTS

Two profiles were selected from the aeromagnetic map (Figure 2) and the Bouguer gravity map (Figure 3) for analysis. These are labeled AA' and BB' in the figures. The regional field was removed from the profiles using a graphical smoothing technique. The profiles were selected to cross as many of the gravity anomalies as possible. All profiles were modeled using standard two dimensional computer modeling techniques adapted for use on a personal computer. The results of the modeling are presented in Figures 4 and 5.

The observed values in each case are denoted by open squares. Both the theoretical curves and the interpreted regional field are shown as solid lines. The initial shapes of the bodies were cho-

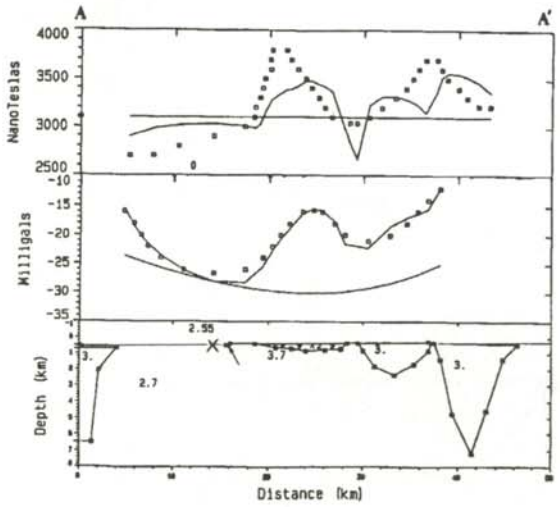

Figure 4
Profile AA'. Magnetic profile (top), gravity profile (center), interpreted geology (bottom). Open squares indicate gravity and magnetic profile data taken from contour maps. Density values in g/cm^3 are printed on the bodies. Unmarked bodies are gabbroic intrusives. Checks indicate ultramafic intrusives. Arrow indicates the hypothesized fault. X indicates intersection of profiles.

sen to be in accord with the body shapes used in other studies of northeast Iowa. The shapes of the source bodies were then modified as necessary to achieve a match with the observed anomalies.

The densities and magnetic susceptibilities used in the computation of the bodies are representative of measured values from Precambrian outcrops and basement drill holes. [11] All magnetic profiles were computed with a remnant magnetization vector having an intensity of .0033 emu/cm^3, declination of 291 degrees and inclination of 38 degrees. [12] These values are typical of Middle Keweenawan age intrusive rocks in Minnesota.

The calculated Bouguer gravity profiles match well, but the calculated magnetic profiles show appreciable deviations from the observed curves at several locations. The inherent ambiguities associated with potential field theory does not justify a detailed fit of the magnetic data. Therefore, no attempt was made to achieve a better fit. Indeed, models obtained from matching observed and theoretical gravity and magnetic anomalies are considered suggestive only. They must be constrained with information from other sources such as geological and drill hole data.

A model was created which took into account the thickness of the Paleozoic sediments as shown on a basement configuration map of Iowa. [13] Existing values for the density and magnetic susceptibilities of olivine cumulate were used. [14] Granite and related rocks are the predominant lithologies found in the basement rocks of the Midwest, therefore, a granitic crust intruded by middle Keweenawan mafic bodies is consistent with previous work.

Profile AA' (Figure 4) shows the granitic crust intruded by an olivine cumulate body and three gabbroic bodies. The Fayette Structural Zone intersects the line of profile AA' about 16 km north of the southern end of the profile (the arrow in Figures 4 and 5). As modeled, the gravity effect of the fault is confined to a small topographic expression at the basement surface

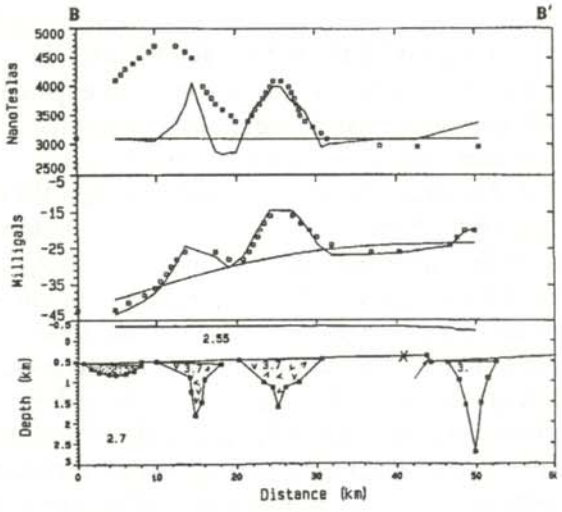

Figure 5
Profile BB'. Magnetic profile (top), gravity profile (center), interpreted geology (bottom). Dots idicate Keweenawan age clastics. Open squares idicate gravity and magnetic profile data taken from contour maps. Density values in g/cm^3 are printed on the bodies. Unmarked bodies are gabbroic intrusives. Checks indicate ultramafic intrusives. The arrow indicates hypothesized fault. X indicates intersection of profiles

because there is no density contrast shown within the deeper crust. Any reasonable amount of vertical displacement of the Precambrian basement does not produce an appreciable gravity anomaly for the modeled density. Therefore, the large gravity anomaly just north of the presumed fault is due primarily to the modeled intrusive bodies and not to the fault or fault zone.

Profile BB' (Figure 5) runs west to east across the survey area. The western most body has been modeled as Precambrian clastics.[15] The two central bodies are modeled as ultramafic olivine cumulate because they have magnetic anomaly intensities similar to the Osborne anomaly located in the southeast portion of the study area (see Figure 2). Further to the east an irregular intrusive mass of gabbroic composition has been modeled.

A comparison of the aeromagnetic and Bouguer gravity anomaly maps (Figures 2 and 3) indicates that the Fayette Structural Zone is not clearly defined on the gravity map. The linear magnetic low associated with the Fayette Structural Zone trends northeast from just south of the Randalia anomaly to the intersection of profiles AA' and BB'. A comparable gravity anomaly does not appear to exist, although some reflection of the fault may well occur just north of the intersection of the profiles AA' and BB' in a steep gradient region that has been related to ultramafic intrusions, juxtaposed against the granitic country rock.

SUMMARY

Figure 6 shows our interpretation of the basement lithology and structure of the study area based on the profiles of Figures 4 and 5 and the aeromagnetic map shown in Figure 2. The interpretation is that of a granitic basement with several mafic and/or ultramafic intrusive bodies and a small clastic basin along the western edge of the study area. The choice of lithologies was based primarily on drill hole information from the surrounding area.

The presumed Fayette Structural Zone is also shown on the map. However, interpretation of the gravity profiles failed to confirm the presence of a fault or the northeastern extension of the fault coincident with the structural zone. Additional modeling is underway to investigate the possibility of an intrusive body emplaced along the presumed fault. Such a model might better satisfy the magnetic data and might also be more consistent with results from other studies of northeast Iowa.

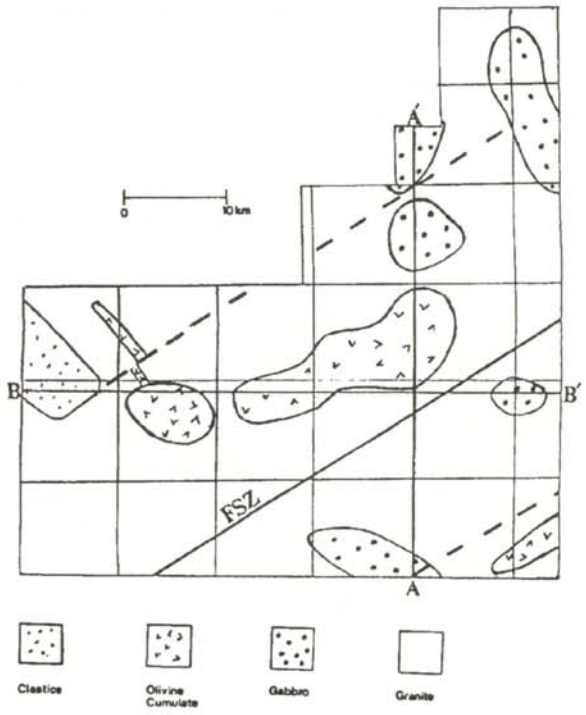

Figure 6
Structural and lithologic interpretation of the survey area. FSZ locates the Fayette Structural Zone as interpreted from aeromagnetic data. Faults inferred from the work of others are indicated by widely spaced dashed lines. The closely spaced dashed line is the possible northeast extenstion of the Fayette Structural Zone.

ACKNOWLEDGEMENTS

The authors wish to thank the Pew Foundation for funding this project. We are also indebted to Raymond Anderson and the Geological Survey Bureau of Iowa for their patient assistance in providing useful data and other information. We would like to thank Joel Kindem for his help with data entry and organization early in this project.

REFERENCES

1. Airborne Magnetometer Survey of Northeast Iowa, 1968, Iowa Geological Survey, p. 26.

2. R.R. Anderson, private communication, 1988.
3. K.L. Kittleson, Gravity Study of the Osborne Magnetic Anomaly, Clayton County, Iowa, unpublished M.S. thesis, University of Iowa, 1975, p. 105.
4. J.L. Gilmore, Gravity Survey of the Randalia Magnetic Anomaly, Fayette County, Iowa, Iowa Geological Survey, Report of Investigation No. 11, 1976, p. 29.
5. J.G. Stepanek, Geological Interpretation of an Aeromagnetic Anomaly near Randalia, Northeastern Iowa, unpublished M.S. thesis, University of Iowa, 1978, p. 113.
6. K.L. Kittleson, op.cit.
7. A. Yaghubpur, Preliminary Geologic Appraisal and Economic Aspects of the Precambrian Basement of Iowa, Ph.D. dissertation, University of Iowa, 1979.
8. W.R. Muehlberger, Re.E. Denison, and Lidiak, "Basement Rocks in Continental Interior of United States", The American Association of Petroleum Geologists Bulletin, , 51, 12, Dec. 1967, pp. 2371.
9. W.J. Hinze, R.L. Kellogg and Meritt, Gravity and Aeromagnetic Anomaly Maps of the Southern Peninsula of Michigan, Department of Natural Resources, Geological Survey Division, Report of Investigations No. 14, 1971.
10. M.B. Dobrin, Goephysical Prospecting, McGraw-Hill Book Co, Inc., 1960.
11. H.M. Mooney and R. Bleifuss, Magnetic Susceptibility Measurements in Minnesota Part II: Analysis of Field Results, Geophysics, 18, 1953, pp. 383-393.
12. C. E. Jahren, Magnetization of Keweenawan Rocks near Duluth, Minnesota, Geophysics, 30, 5, 1965, pp. 858-874.
13. R.R. Anderson, personal communication.
14. K.L. Kittleson, op.cit.
15. J.L. Gilmore, op.cit, J.G.Stephanek, op.cit.

GLOSSARY

Structural Zone: A linear trend produced by deformation or displacement of rocks by faulting or intrusion of igneous rocks.

Gravity or magnetic anomaly: A variation in the gravity or magnetic field caused by a horizontal departure in subsurface density or magnetic susceptibility of subsurface rock formations from a smooth regional variation.

Basement: The series of igneous and metamorphic rocks generally underlying the oldest fossiliferous stratified sedimentary rocks of the region.

Fault: A surface along which rocks have been broken and offset. A basement fault is one that offsets the basement rocks. It may or may not offset the overlaying sedimentary rocks.

Paleozoic: an era of geologic time extending from the end of the Precambrian to the the Mesozoic era, or from about 570 to about 225 million years ago.

Sedimentary rock: A rock derived from pre-existing rocks through the action of weathering, erosion, transportation and deposition.

Mafic rock: An igneous rock containing more than 50% ferromagnesiam (high in iron and magnesium) minerals. Ultramafic rock is composed entirely of ferromagnesian minerals.

Gabbro: A dark-colored, coarse grained, mafic, igneous rock composed of minerals high in iron and magnesium which was intruded beneath the surface. Some gabbros are exceptionally rich in iron and magnesium; these are called olivine gabbro or olivine cumulate gabbro. The extrusive equivalent of gabbro is basalt.

PreCambrian: All geologic time and its corresponding rocks, before the beginning of the Paleozoic. It is equivalent to about 90% of geologic time.

Lithology: The science dealing with the composition and structure of rocks.

Gravity station: A place with known elevation, where the gravity value is measured. The station is occupied by taking a gravity meter to the site and measuring the gravity value relative to a base station where the absolute gravity has been determined by a pendulum measurement or other techniques.

Igneous rock: Rocks formed by cooling and solidification of a once molten material called magma. The magma always intrudes into older rocks.

Clastic sediment: A sedimentary rock, formed by the accumulation of fragments derived from pre-existing rocks.

FACULTY SPONSOR

Dr. Richard L. Kellogg
Physics Department
Luther College
Decorah, IA 52101

THE FRICTION AND WEAR PROPERTIES OF DIAMOND-LIKE CARBON FILMS *

Michelle S. Switala
Franklin and Marshall College
Lancaster, PA 17604

ABSTRACT

The friction properties of diamond-like carbon (DLC) coatings have been examined. These thin solid films were deposited on the following ceramics: silicon nitride, silicon carbide and zirconium oxide. Pin-on-disk machine tests were performed on coated and uncoated samples as well as the following standards: amorphous carbon, pyrolytic graphite and natural diamond. The coefficient of friction and wear were measured using parameters of load and environment. The results from the DLC films were compared with the other tested materials. Proposed mechanisms for the frictional behavior were examined and a new one introduced. Raman spectroscopy was used to confirm the conclusions. In all cases, the friction and wear results of the DLC were superior to any other material used.

INTRODUCTION

Scientists have been fascinated by the superior properties of natural diamond: high hardness, high refractive index, high thermal conductivity, high electrical resistivity, optical transparency, chemical inertness and radiation resistance. [1-5] Tribologists have attempted to utilize the excellent friction and wear properties of natural diamond, but natural diamond is expensive and difficult to mold or apply. These limitations forced scientists to search for a substance that has mechanical properties similar to natural diamond, but is easier to work.

Forty years ago, a special type of thin solid film produced by deposition was invented. It had a molecular structure close to natural diamond and very similar mechanical properties. This easily produced film was named Diamond-Like Carbon (DLC). Some of the methods used to make these films include ion beam deposition, ion beam assisted deposition, chemical vapor deposition and radio frequency discharge.

These films are currently used in places where other lubricants, such as oil, grease and graphite fail. The Navy coats precision guidance bearings where oil and grease can contaminate, leak and cause unwanted torque that interferes with signal processing. [6] When DLC is applied to ceramic cutting tools, the coefficient of friction is five times lower than that of uncoated blades and the wear is ten to one hundred times less. [7] Since DLC has a dielectric constant between 8 and 14, capacitors and p-n junctions which use DLC are excellent. [8,9]

This paper is a study of the frictional properties of these revolutionary DLC using a pin-on-disk machine. The frictional properties dependence on three different parameters were examined: load, environment and rubbing (counterface) material. The tests were duplicated on uncoated samples, natural diamond, pyrolytic graphite

---

Miclelle graduated in the spring from Franklin and Marshall College with a B.A. in physics. This summer, she taught physics labs for Johns Hopkins University's Center of Talented Youth program for the third year. Michelle will attend the University of Arizona for her Ph. D. in physics, probably concentrating in optics.

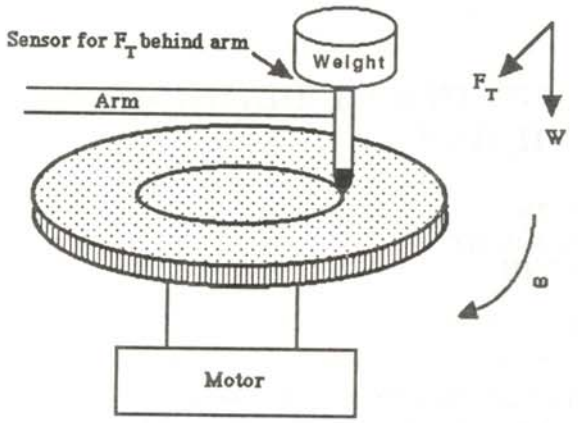

Figure 1
Schematic diagram of the CSEM Pin-on-disk machine used for measuring frictional coefficient.

and amorphous carbon. Analysis of the friction results, coupled with a comparison to standards and analysis of Raman spectra, has led us to propose a new mechanism to describe the frictional behavior of DLC.

THEORY

The friction between two rubbing surfaces depends upon the true area of contact, the interfacial bonds and the deformation process. [10] Each of these properties is affected when a thin solid lubricating film is deposited on one of the surfaces. Elastic films obey the following relationship between the true area of contact and the load:

$$A = k\,W \qquad (1)$$

where A is the true area of contact, k a proportionality constant and W is the load. Thin solid films shield rubbing materials from interfacial Van der Waals forces. Finally, films affect the deformation process by changing the shearing mechanism of the substrate. [11]

In general, an applied load acting tangential to an interface causes a shear stress. The tangential force, opposite in direction to the frictional force, is directly related to this shear stress (s) and the true area of contact:

$$F = A\,s \qquad (2)$$

Large frictional forces arise when either the area of contact is large or the shear stress is large.

The DLC films reduce the friction between two rubbing materials in a slightly different manner than most thin films. The DLC is probably elastic, as natural diamond [12], and thus supports the counterface material well by only allowing a small area of contact. The material that is rubbed over the filmed substrate may never sink to touch the substrate at all. [13] The shearing involved during the rubbing would then be interfacial rather than inter-film. If the rubbing material sank into the DLC film, the DLC's moderate shear strength would give rise to a high coefficient of friction. The apparently low contact adhesion of the films also indicates an interfacial shear. [14]

Because the shear is thought to be interfacial, the molecular structure of the film surface becomes very important. If the surface structurally appears as graphite, then the film may, as with graphite, have a lower coefficient of friction in humid environments. Different molecular surfaces behave differently in dissimilar conditions. Thus, the structure of the film must be assessed before accurate mechanisms for producing friction can be proposed.

Measurements of the coefficient of friction as a function of load can show if the film is elastic. The coefficient of friction of elastic contacts decreases as the load is increased because the coefficient of friction is inversely related to the Hertzian pressure, which is proportional to the cube root of the load. [15]

The wear mechanism, related to the strength of the film, is more difficult to identify. The wear rate depends on the hardness [16] and the surface roughness of the second member. [17]

The results of the coefficient of friction and wear rate tests under the load, environment and ball material parameters should confirm elasticity, hardness and shear strength. These results, coupled with the information about the molecular structure revealed by Raman spectroscopy,

should allow us to devise an accurate picture of the film.

THE EXPERIMENT

The DLC samples were prepared at Colorado State University.[18] The Si_3N_4, SiC and ZrO_2 disk samples (3 in. diameter) were cleaned with acetone and placed in an ion beam deposition vacuum chamber. They were sputter cleaned in a 1keV argon beam for 3 minutes before coating to a thickness of approximately 2 μm at an energy of 400 V. The samples were cooled with water. Since the DLC does not adhere well to $Zr0_2$, these disks were coated with approximately 30-50 nm of SiC before being coated with DLC.

Before testing, the DLC, pyrolytic graphite and amorphous carbon samples were not cleaned because the ultrasonic cleaning might have disrupted the smooth surfaces. The uncoated discs, all of the balls and the diamond pin were degreased.

All of the tests were performed on a pin-on-disk machine (see Figure 1). A rectangular plexiglass cover was fitted over the pin-on-disk machine permitting various environments to be created. The cover had a sensor for relative humidity and temperature. The temperature was approximately 27 C in all cases. The relative humidity for the various atmospheres was:

Atmosphere	Humidity in %
Argon	0
Nitrogen	0
Dry Air	1.9 ± 2
Normal Air	48 ± 10
Humid Air	90 ± 3 .

The environment was prepared and allowed to stabilize before any tests were begun.

In all but one case, the total number of revolutions of the disk was set to keep the sliding distance constant at 165 m. and the motor set to have a sliding speed of 2.6 cm/s. Since we did not have a diamond disk to compare to the DLC disks, we rubbed a diamond pin on an uncoated

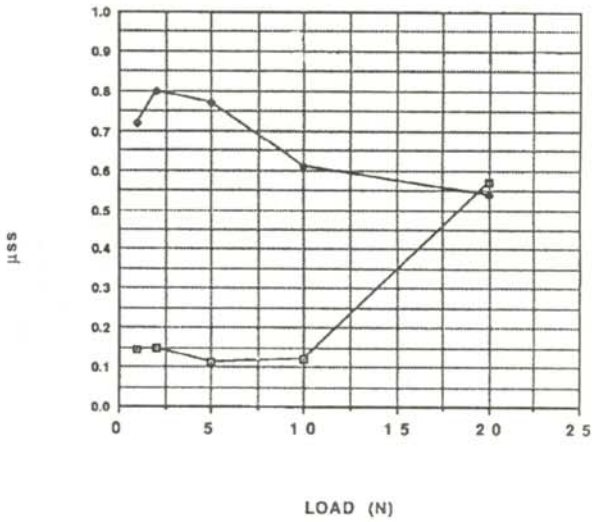

Figure 2
Steady state coefficient of friction versus load for DLC coated (open squares) and uncoated (solid squares) Si_3N_4 in a normal environment.

Si_3N_4 disk. The same spot on the pin would be rubbed through out the test unlike the DLC disk, so the sliding distance was reduced to 82 m. to achieve more equal testing circumstances. In all tests, the coefficient of friction was measured in the 'steady state', when the value of the coefficient had reached an approximately constant value.

DATA AND RESULTS

The first tests, shown in Figure 2, examine the performance of the DLC's compared to uncoated samples. From 1 to 10 N., the coefficient of friction decreases with increasing load as predicted for elastically loaded contacts. At 20 N., the film appears to break down, as seen by the sharp increase in the steady state coefficient of friction.

Figure 3 shows the dependence of the coefficient of friction on relative humidity. Once again, the film tested in the normal environment was stable until loaded to 20 N.

Figure 4 displays the friction properties of DLC with other similar materials with possibly similar molecular structure. Raman spectroscopy (see Figure 6) reveals that there is significant sp^2 bonding (associated with graphite) in DLC

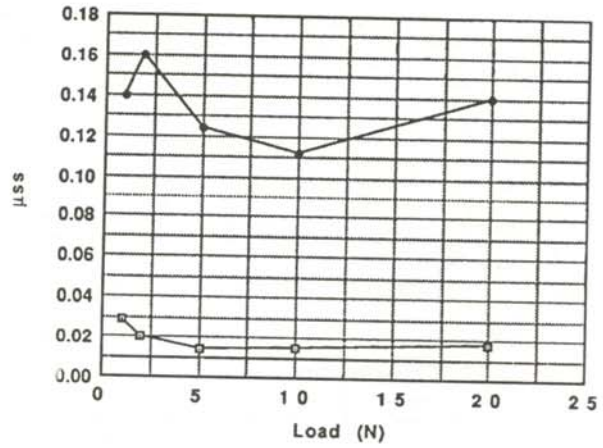

Figure 3
Steady state coefficient of friction versus load for argon (open squares) and normal (black squares) environments done with a sapphire ball on DLC ZrO_2.

films, but the friction characteristics of graphite are inverse to those of DLC. The coefficient of friction for graphite decreased under humid circumstances, while the DLC films performed best under completely dry conditions. Natural diamond was the only material which had the same dependence of frictional coefficient on humidity as the DLC film.

The wear rate (WR) was determined by first measuring the diameter of the wear scar under an optical microscope. The wear was calculated using the equation:

$$W = \pi d^4 / (64 r) \qquad (3)$$

where d is the diameter of the scar and r is the radius of the ball. The wear rate was found by dividing the wear by the load and the sliding distance. Only the wear of the balls was measured, because the DLC films showed no measurable wear. They were smooth to approximately 64 nm. The films seemed to simply polish more.

Figure 5 shows the wear rate (WRb) for the different environmental conditions. The wear rate of DLC appears similar to that of amorphous carbon.

Figure 6 is the Raman specta of the DLC ZrO_2 disk under several different conditions. The spectrum, taken from an unworn spot on the disk, shows a peak at 1334 cm^{-1} which represents sp^3 bonding, the tetrahedral bonding found in diamond. In natural diamond, this peak is normally found at 1330 cm^{-1}. This peak can be significantly shifted when the sp^3 bonds are subjected to conditions which cause internal stress. [19] Ions impinging on the substrate surface during the DLC formation possess so much energy that they cause localized temperature and pressure spikes of large enough magnitude to collapse the carbon atoms into tetrahedral structure. [20]

Sp^2 bonding, asociated with graphite, is also apparent as the broad hump centered at 1594 cm^{-1}. The width of the sp^2 peak can be as large as 200 cm^{-1} [21] for two reasons: the material contains a few different carbon structures [22] and Raman peaks become less sharp as the number of grain boundaries increases. Many boundaries indicate small grain size. The shift of this broad peak from the single crystal graphite line at 1580 cm^{-1} also indicates the presence of small grains of graphite. [23] The absence of the polycrystaline graphite peak at 1355 cm^{-1} implies that the film contains no graphite domain size at all [24]. This contradiction can be resolved if the sp^2 bonds are dispersed within the crystal rather than in a spatially separated phase. [25]

The other lines shown in Figure 6 are Raman spectra of wear tracks produced in humid, nor-

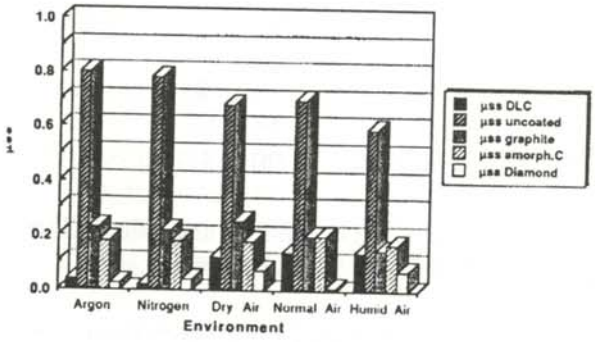

Figure 4
Steady state coefficient of friction versus environment for Si_3N_4 on DlC and uncoated SiC with a 2 N. load.

mal and dry environments. The broad sp^2 peak increased in size in all environments. When diamond structure is stressed, the sp^2 regions increase. [26] The shifting of the diamond line (from 1334 cm^{-1} to 1336 cm^{-1}), indicating internal stress, implies that the sp^3 bonds in the film must be affected in water-rich environments.

PROPOSED FRICTION/WEAR MECHANISMS

The suggested structure of the DLC is 2/3 tetrahedral and 1/3 trigonal in coordination. [27,28] It is proposed that the films are puckered n-fold carbon rings ($3 \leq n \leq 8$) of hexagonal or pentagonal character which are connected by cross links in which tetrahedral bonding is observed.[29]. Such a structure would explain why the DLC films have a lower density than graphite, but properties similar to those of natural diamond.

Several mechanisms have been proposed to explain the special frictional and wear behavior of the DLC coatings. Figure 7 shows an adhesion mechanism that best explains our results. Dangling hydrogen atoms, satisfying and stabilizing open surface carbon bonds left during DLC film deposition, [30,31] do not bond strongly to the ball material, so very little friction is seen in inert environments. When water vapor (thus oxygen) is introduced into the environment, the dangling hydrogens form surface water groups.[32] The

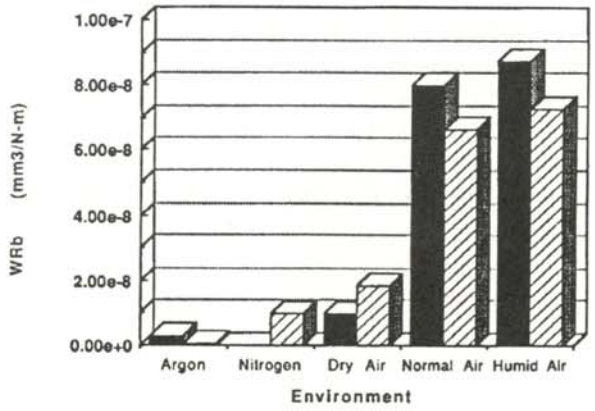

Figure 5
Ball wear rate (WRb) versus environment for amorphous carbon (solid black bars) and DLC (striped bars) with a 2 N. load.

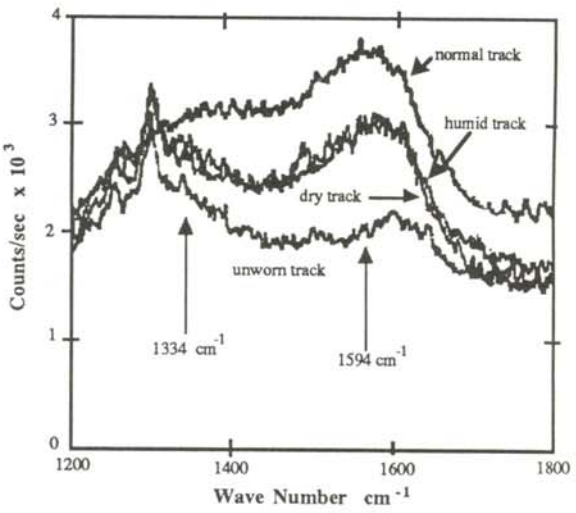

Figure 6
Raman spectra for DLC for unworn, humid, normal and dry environment wear tracks.

water groups are adhesive, as evidenced by the increase in the coefficient of friction in dry, normal, and humid environments over the argon and nitrogen environments. The formation of water groups in the first three environments explains the similarities in the Raman spectra for the corresponding wear tracks. The oxygen concentration in exposed samples was found to be 1.5 times higher than unexposed samples, [33] also suggesting the formation of surface water groups in water-rich environments.

This study tested the performance of DLC films under various loads and in various environments. Further studies need to be performed to reveal the film's behavior in a range of temperatures. The DLC films are not perfect diamonds, but since they exhibit nearly the same properties, they are easily formed and they seem to adhere well, they may exceed natural diamonds for certain applications.

ACKNOWLEDGEMENTS

The author was a participant in the Fall 1990 Science and Engineering Research Semester coordinated by the Division of Education Programs at Argonne National Laboratory. She would like to thank Dr. Ali Erdemir and Dr. Fred Nichols at Argonne National Laboratory

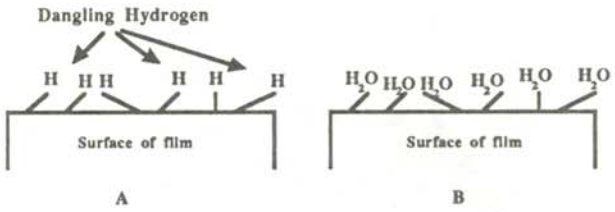

Figure 7
A) Hydrogen rich DLC surface, showing dangling hydrogen atoms.
B) The hydrogen rich DLC surface in a humid environment

for their valuable help.

REFERENCES

* Work performed at Argonne National Laboratory, a contract laboratory of the United States Department of Energy.

1. H. Tsai and D.B. Body, J. Vac. Sci. Technol. A, 5, 6, 1987, p. 3288.
2. J.E. Sundgren and H.T.G. Hentzell, J. Vac. Sci Technol. A, 4, 5, 1986, p. 2259.
3. S. Aisenberg and R. Chabot, J. Appl. Phys.,43, 7, 1971, p. 2955.
4. N.N. Greenwood and A. Earnshaw, Chemistry of the Elements, Pergamon Press, NY, 1984, p. 307.
5. S.C. Sharma, et. al., J. Mater. Res., 5, 11, 1990, p. 2424.
6. I.L. Singer, Mat. Res. Soc. Symp. Proc., 140, 1989, p. 215.
7. S. Aisenberg and R. Chabot, J. Vac. Sci. Technol., 10, 1973, p. 104.
8. H. Tsai and D.B. Body, J. Vac Sci. Technol. A, 5, 6, 1987, p. 3290.
9. S. Aisenberg and R. Chabot, J. Appl. Phys., 42, 7, 1971, p. 2955.
10. D. Tabor, Transactions of the ASME, J. Lub. Technol. 103, 1981, p. 170.
11. Ibid. p. 174.
12. F.B. Bowden, et.al., Proc. R. Soc. London, 208, 1951, p. 454.
13. Ibid.
14. I.L. Singer, Mat. Res. Soc. Symp. Proc. 140, 1989, p. 216.
15. R. Roark and W. Young, Formulas for Stress & Strain 5th Ed., McGraw Hill Book Co, 1975 pp 513 - 522.
16. D. Crompton, Proc. R. Soc. London, A, 33, 1973, p. 435.
17. M. Kohzaki, Mat. Lett., 9, 2-3, 1990, p. 82.
18. Sample prepared by R. Wei and P. Wilbur at Colorado State University, Deprtment of Mechanical Engineering.
19. L.H. Robins, et. al., J. Mat. Res., 5, 11, 1990, p. 2459.
20. C. Weissmantel, et. al., Thin Solid Films, 79, 1980, p. 19.
21. L. H. Robins, op. cit. p. 2457.
22. Ibid.
23. F. Tuinstra, and J.L. Koenig, L. Chem. Phys., 53, 1970, p. 1126.
24. Ibid.
25. L.H. Robins, op. cit., p. 2465.
26. C. Weissmantel, et. al., Thin Solid Films, 96, 1982, p. 39.
27. C. Weissmantel, et. al., Surf. Sci., 86, 1979, p. 207.
28. J. Flink, et. al., Solid State Commun., 47, 1983, p. 687.
29. L.H. Robins, op. cit., p. 2465.
30. C. Weissmantel, et al., Thin Solid Films, 96, 1982, p. 39.
31. D.E. Peebles and L.E. Pope, J. Mat. Res., 5, 11, 1990, p. 2592.
32. K. Miyoshi, et. al., Mater. Sci. Forum, 52/53, 1989, p. 645.
33. Y. Kokaku and M. Kitoh, J. Vac. Sci. Technol, A, 7, 3, 1989, p. 2313.

FACULTY SPONSOR

Dr. Fred Nichols
Tribology, Materials and Components Tecchnology Division
Argonne National Laboratory, Bldg. 212
9700 South Cass Avenue
Argonne, IL 60439-4838.

TEMPERATURE AND HOST DEPENDENCIES OF DIVALENT EUROPIUM IONS IN A CRYSTALLINE ENVIRONMENT

Mark Jurena *
Division of Earth and Physical Sciences
The University of Texas at San Antonio
San Antonio, TX 78285

ABSTRACT

The optical absorption studies of Eu^{2+} embedded in different host lattices: NaCl, KCl and $RbMgF_3$ have been performed in liquid nitrogen, dry ice and room temperatures. The crystal field splitting are quite prominent in NaCl and KCl lattices. On the other had, the $RbMgF_3$:Eu^{2+} absorption shows only one broad band without any trace of structure even at lower temperatures. The NaCl:Eu^{2+} absorption at dry ice and liquid nitrogen temperate exhibits clear structures.

INTRODUCTION

This study was performed on various types of crystals to determine their potential as solid state laser materials. There is a need for tunable solid state lasers covering new spectral ranges to augment the titanium sapphire laser. Such a laser would have applications in both industrial and medical research.

Tunable solid state lasers would also be of immense help in spectroscopic measurements and have numerous advantages over organic dye lasers. For example, they would eliminate the painstaking precautionary measures necessary to keep the dye system free from any contamination.

The primary characteristics of materials that would be suitable for a tunable solid state laser are broad and intense regions of absorption as well as emission. These lines must also have suitable electronic transition lifetimes. From an economic point of view, it would be desirable that these materials have the strong absorption and emission at room temperature. Once we have a strong emission spectrum covering a wide range of electromagnetic waves, we can tune the laser at desired wavelengths using a grating and other optical accessories. Since strong emission also implies strong absorption, a thorough characterization of optical absorption of a material helps to determine if it can be useful as material for a tunable solid state laser.

The crystals used in these absorption experiments were divalent Europium doped $RbMgF_3$, NaCl and KCl. These crystals contain monovalent donor elements. All of the crystals are cubic in structure, while the $RbMgF_3$ has the tendency to have a cubic structure with corners that are not orthogonal to each other. [1] The $RbMgF_3$ has a perovskite structure. [2]

In all three crystal hosts, each monovalent ion (Na^+. K^+ and Rb^+) is replaced by divalent Eu^{2+} during crystal growth. This leaves a cation vacancy for every ion doping, which is illustrated in Figure 1. The measurements performed on these crystals entail determining the ultra-violet absorption at different temperatures. The lowering of the temperature is expected to

---

Mark received his B. Sc. in physics from the University of Texas at San Antonio. He is currently a graduate student in mechanical engineering at the University of Texas at San Antonio.

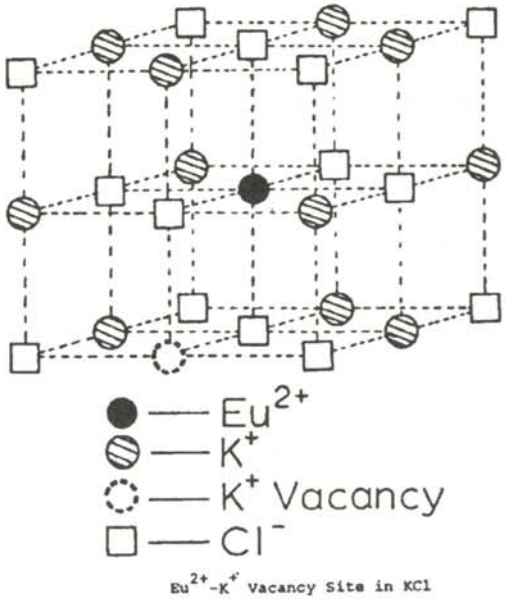

Figure 1
Doping process and structure of KCL:Eu^{2+}.

increase the absorption peaks while the bands become narrower. [3]

In all of the materials studied, Eu^{2+} has intense absorption bands in the visible and near ultraviolet regions of the spectra . These absorption bands are associated with the electric dipole allowed transitions between the $4f^{n-1}$ and 5d configurations. The Eu^{2+} 5d electron-lattice interactions result in broad bands and an intense absorption that is dependent on the crystal host.[4]

EXPERIMENTAL PROCEDURE

All of the absorption data were taken using a Cary-14 spectrophotometer which was updated with a modified electronics to interface to a computer. The computer contained a number of programs for data gathering and analysis. For this project, only the data gathering section of the software was used.The data were gathered with the crystals mounted in a liquid nitrogen cryostat. The temperature measurements were made with a digital thermometer hooked up to a K-type thermocouple. The measurements were taken over the space of several days.

The crystals were mounted in the cold finger of the cryostat and masked so as to prevent any stray light from going around the crystal without passing through it. The cryostat was then sealed and evacuated with a roughing pump for 8 hours to obtain a vacuum of about 10^{-4} Torr. The cryostat was then placed in the Cary-14 and sealed to prevent any stray light from entering the specimen chamber. The digital thermometer was then connected to the cryostat. Absorption data at room temperature (300 K), dry ice temperature (200 K) and liquid nitrogen (80 K) temperature were recorded on a floppy diskette. The optical absorption data, optical density vs. wavelength, were then transferred to a PC which converted the optical density to absorption coefficient and finally, the data were plotted as absorption coefficient vs. wavelength.

RESULTS AND DISCUSSION

Figure 2 illustrates the host and temperature dependent absorption data for Eu^{2+}. The KCl:Eu^{2+} data show two distinct peaks, characteristic of crystal field splitting, one at approximately 240 nm. and the other at approximately 330 nm. These 330 nm. peak does show fine structure. The $RbMgF_3$:Eu^{2+} absorption data exhibit a strong broad band of absorbance ranging from 230 nm. to 330 nm. There is an almost total absence of fine structure in these results. But fine structure and crystal field splitting are evident in the NaCl:Eu^{2+} absorption data. The two peaks at 260 nm. and at approximately 340 nm. are characteristic of the crystal field splitting. The peak at 260 nm at room temperature has the hint of shoulders on either side of the peak. Fine structure for the peak near 340 nm is not as prevalent.

The most noticeable difference among the various absorption spectra was that when all the samples were cooled, the peak intensities were higher and the Full Width at Half Maximum (FWHM) decreased. Fine structure also began to appear clearly around the 330 nm peak of KCl:Eu^{2+} .

The main difference between the two salts and the perovskite crystal is the existence of hyper-

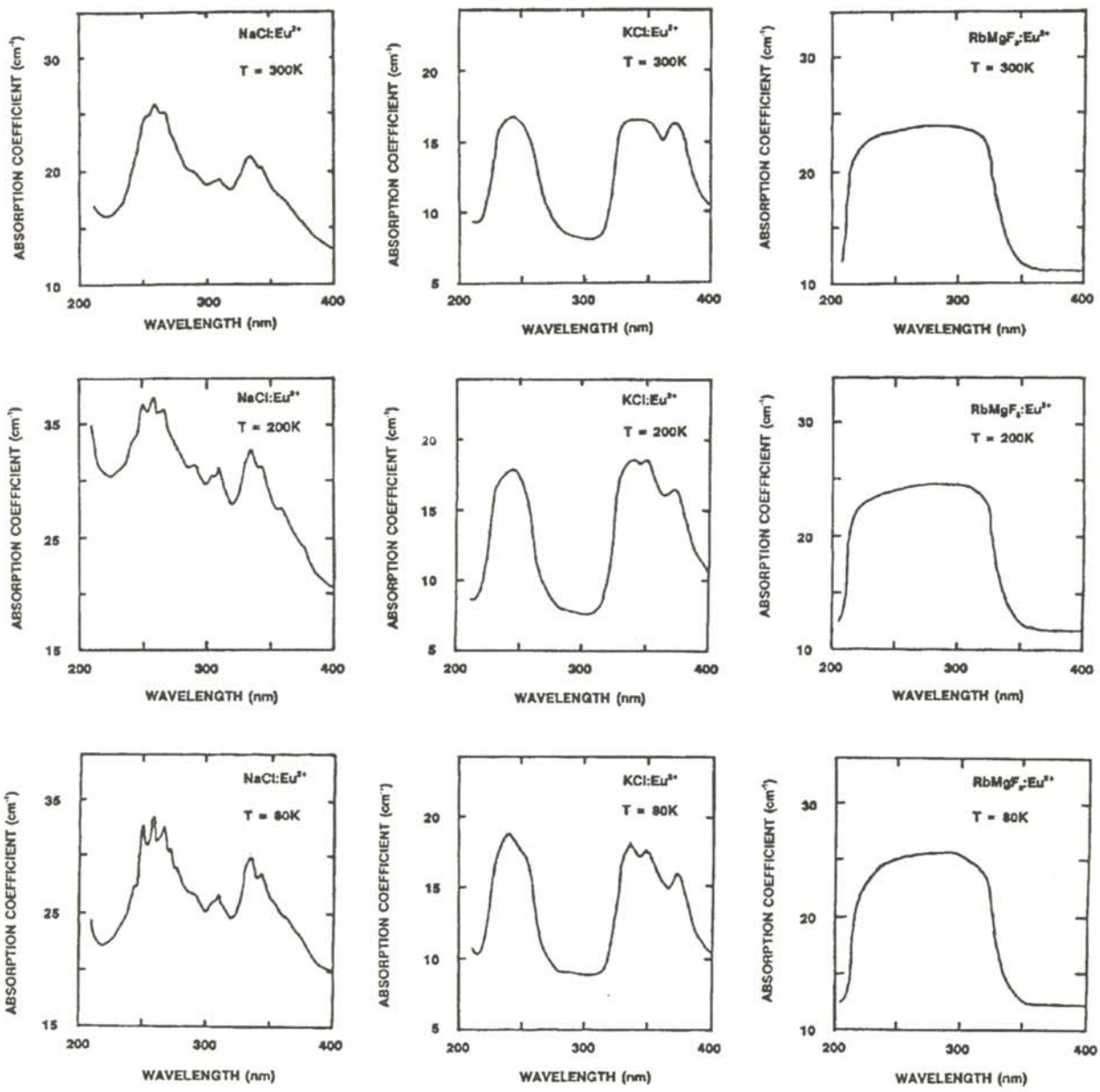

Figure 2

Host and temperataure dependent absorption spectra of Eu^{2+}.

fine structure in the salts. NaCl:Eu^{2+} and KCl:Eu^{2+} display the two distinct peaks while $RbMgF_3$:Eu^{2+} just shows a broad absorption band. These general features continue as the sample is cooled. The appearance of fine structure with decreasing temperature is most noticeable in the shorter wavelength peak for NaCl:Eu^{2+} and to a lesser degree in the longer wavelength peak of KCl:Eu^{2+}. There is no apparent fine structure in the $RbMgF_3$:Eu^{2+} data even as the temperature is lowered.

SUMMARY

$RbMgF_3$:Eu^{2+} with its broad band (FWHM) and high peak absorption shows a potential for use as a tunable solid state laser. Although NaCl:Eu^{2+} has a slightly higher peak absorbance than $RbMgF_3$:Eu^{2+}, it has a much narrower FWHM and like KCl:Eu^{2+}, exhibits fine structure.

The next step in determining the suitability of the crystal for use in a solid state laser would be to obtain the emission spectra. Life-time measurements would also be needed to determining the quantum efficiency of the materials.

ACKNOWLEDGEMENTS

The author would like to thank his advisor, Dr. Dihraj K. Sardar for his assistance and encouragement throughout this project. He would also like to thank Dr. Robert Renthal for the use of the spectrophotometer in his lab. This work was supported by NSF Grant No. DMR-8900834.

REFERENCES

1. C. Kittel, Introduction to Solid State Physics, 6th Ed., John Wiley, NY, 1986, p. 406.
2. J. Garcia and W.A. Sibley, "Energy Transfer Between Europium and Manganese Ions in Fluoroperovskite Crystals", Journal of Luminescence, 42, 1988, p. 109.
3. N Koumvakalis, W.A. Sibley and G.E. Venikous, "Thermal Dependence of Impurity Induced Fluorescence in the System $RbMgF_xMn_{1-x}F_3$", Journal of Luminescence, 15, 1977, p. 283..
4. R. Alcala, D.K. Sardar and W.A. Sibley, "Optical Transitions of Eu^{2+} Ions in Crystals"' Journal of Luminescence, 27, 1982, p. 273.

FACULTY SPONSOR

Dr. Dhiraj Sardar
Divison of Earth and Physical Sciences
The University of Texas at San Antonio
San Antonio, TX 78285-0663

A HAMILTONIAN FOR GEOMETRICAL OPTICS

Brian N. Turner
Southern Nazarene University
Bethany, OK 73008

ABSTRACT

Since both geometrical optics and mechanics can be derived from variational principles (Fermat's principle and Hamilton's principle respectively), we assume a mechanical analogy for geometrical optics and derive a 'Newtons second law' , the Lagrangian and the Hamiltonian for geometrical optics. We show that these results are consistent with Hamilton's equations and the Hamilton-Jacobi equation. The theory is used to work out some classical examples in geometrical optics, such as Snell's law.

INTRODUCTION

FERMAT'S PRINCIPLE

Geometrical optics can be derived from a variational principle called Fermat's Principle: Of all possible trajectories that a light ray might follow going between two fixed points (a and b), the trajectory actually followed is the one for which the elapsed time is a minimum:

$$\delta\int_a^b dt = 0 . \tag{1}$$

Using the relationship between the speed of light c and the definition of velocity

$$v = \left| \frac{d\mathbf{r}}{dt} \right| = \frac{c}{n(\mathbf{r})} , \tag{2}$$

where $n = n(\mathbf{r})$ is the index of refraction, Equation 1 becomes:

$$\delta\int_a^b n(\mathbf{r}) \, |d\mathbf{r}| = 0 . \tag{3}$$

Brian is from the Kansas City area. He graduated from Southern Nazarene University in May 1991, and has begun graduate studies at the University of Texas at Dallas, where he plans to study relativity.

Introducing an arbitrary parameter s, Fermat's Principle can be written as:

$$\delta\int_{s(a)}^{s(b)} n(\mathbf{r}) \left| \frac{d\mathbf{r}}{ds} \right| ds = 0 . \tag{4}$$

This is a variational problem where a functional (L) is being made an extremum:

$$\delta\int_{s(a)}^{s(b)} L \, ds = 0 , \tag{5}$$

where

$$L = L(x_i, x_i') = n(x_i) \, (x_i' \, x_i')^{\frac{1}{2}} = n(x_i) \, r' , \tag{6}$$

where x_i denotes a generalized coordinate or component of $\mathbf{r}$, and the primes denote differentiation with respect to s. Repeated indices are to be summed. This variational problem results in the Euler-Lagrange equation:

$$\left(\frac{\partial L}{\partial x_i}\right) - \frac{d}{ds}\left(\frac{\partial L}{\partial x_i'}\right) = 0 , \tag{7}$$

which becomes, when L from Equation 6 is substituted in it:

$$\mathbf{r}' \nabla n = \frac{d}{ds}\left(\frac{n\,\mathbf{r}'}{r'}\right). \qquad (8)$$

So, the equivalent Lagrangian for geometrical optics is:

$$L = n\,r' \,. \qquad (9)$$

Now, let us find the equivalent Hamiltonian for geometrical optics. The canonical momenta are:

$$p_i = \frac{\partial L}{dx_i'} = \frac{n\,x_i'}{r'} \,. \qquad (10)$$

The Hamiltonian follows from the Legrendre transformation:

$$H = x_i'\,p_i - L \,, \qquad (11)$$

where the x_i' are to be eliminated in favor of the p_i using Equation 10. However, suppose we find the numerical value of H by retaining in Equation 11 the 'generalized velocities' (i.e. x_i'). We find that:

$$H = x_i'\left(\frac{n\,x_i'}{r'}\right) - n\,r' = n\,\frac{r'^2}{r'} - n\,r' = 0 \,. \qquad (12)$$

The numerical value of the Hamiltonian for geometrical optics vanishes!

$$H = 0 \,. \qquad (13)$$

HAMILTON'S PRINCIPLE

The trajectory of a particle of mass m, moving in a conservative field with potential energy $V(\mathbf{r})$, is:

$$\delta\int_a^b \{\, K - V(\mathbf{r}) \,\}\, dt = 0 \,, \qquad (14)$$

where K is the kinetic energy:

$$K = \frac{1}{2}\, m\, \left|\frac{d\mathbf{r}}{dt}\right|^2 . \qquad (15)$$

The Euler-Lagrange equation then becomes:

$$-\nabla\, V(\mathbf{r}) = m\,\frac{d^2\mathbf{r}}{dt^2} \,. \qquad (16)$$

The canonical momenta are:

$$p_i = \frac{\partial L}{\partial \dot{x}_i} = m\,\dot{x}_i = m\,\frac{dx_i}{dt} \,. \qquad (17)$$

The Hamiltonian is defined as:

$$H(\mathbf{r},\mathbf{p}) = p_i\,\dot{x}_i - L = \frac{p^2}{2m} + V(\mathbf{r}), \qquad (18)$$

which is numerically equal to the total energy E:

$$E = K + V \,. \qquad (19)$$

THE MECHANIZATION OF GEOMETRICAL OPTICS

Given that both geometrical optics and particle mechanics can be derived from variational principles and both have their respective Lagrangians and Hamiltonians, can problems in geometrical optics be mapped into corresponding mechanics problems? In other words, can

$$\mathbf{r}' \nabla n = \frac{d}{ds}\left(\frac{n\,\mathbf{r}'}{r'}\right) \qquad (20)$$

be made mathematically equivalent to Newton's second law by putting Equation 20 into the form

$$-\nabla U(\mathbf{r}) = \frac{d^2\mathbf{r}}{ds^2} \qquad (21)$$

for some 'optical potential energy' $U(\mathbf{r})$?

Assuming that such a correspondence exists, we define the 'optical kinetic energy' K to be:

$$K = \frac{1}{2}\,\left|\mathbf{r}'\right|^2 \qquad (22)$$

The value of the 'optical potential energy' is then determined from the Lagrangian:

$$L = K - U \qquad (23)$$

where $L = nr'$. In addition, let us require that numerically

$$H = K + U = 0 \qquad (24)$$

Putting Equation 22 into Equation 24 gives the numerical value:

$$U = -\frac{1}{2}(r')^2 . \qquad (25)$$

However, U is a function of **r**, not **r'**, so to obtain the function U(**r**), we turn to the Lagrangian of Equation 23. Substituting Equation 25 into Equation 23 gives:

$$nr' = \frac{1}{2}(r')^2 - \left[-\frac{1}{2}(r')^2\right] = (r')^2 . \qquad (26)$$

So, if $r' \neq 0$, then numerically

$$n = r' , \qquad (27)$$

where as a function, n depends explicitly on **r**. Substituting Equation 27 into 25 gives the 'optical potential energy' as:

$$U(\mathbf{r}) = -\frac{1}{2}n^2(\mathbf{r}) . \qquad (28)$$

Finally, note that if Equation 27 is substituted into Equation 20:

$$n\,\nabla n = \frac{1}{2}\nabla n^2 = \frac{d\mathbf{r}'}{ds} , \qquad (29)$$

or:

$$-\nabla U = \frac{d^2\mathbf{r}}{ds^2} . \qquad (30)$$

So now, geometrical optics looks formally like the classical mechanics of a particle. In geometrical optics one may form the 'potential energy function' from the refractive index n(**r**) and treat it as the potential energy function in a Newtonian mechanics problem, with the mass replaced by 1 and the time t replaced by s.

'F = ma optics' was discussed by Evans and Rosenquist in a paper of that title [1]. They used a different approach. The authors noticed that if n were set equal to r' in the Euler-Lagrange equation (Equation 20), the differential equation for the ray trajectory would be mathematically similar to F = ma. Evans and Rosenquist imposed n = r' to obtain the desired analogy.

Our approach has been the reverse. We assumed the existence of the mechanical analogy and 'derived' n = r'. Along the way, we also raised the issue of the Hamiltonian dynamics of geometrical optics which was not discussed by Evans and Rosenquist. We shall further develop the Hamiltonian approach in the next section.

The second result is that s is less arbitrary than it was when initially introduced in Equation 4. The constraint n = r' can be inverted into:

$$s = \int \frac{dr}{n} + \text{constant} . \qquad (31)$$

If the integral is evaluated along the ray, then the only arbitrariness in s is the arbitrary integration constant in equation 31. This procedure is analogous to fixing the gauge in a gauge theory. One might say that the Evans-Rosenquist procedure 'fixes the gauge at the outset', while in our procedure, the 'gauge-fixing' arises from the assumption of the existence of the mechanical analogy.

HAMILTONIAN METHODOLOGY FOR GEOMETRICAL OPTICS

Hamilton's equations and the Hamilton-Jacobi equation provide a consistency check on the Hamiltonian for geometrical optics. Hamilton's equations:

$$p_i' = -\frac{\partial H}{\partial x_i} \qquad x_i' = \frac{\partial H}{\partial p_i} . \qquad (32)$$

at first glance seem to imply that the mechanization of geometrical optics is inconsistent. If H = 0, then Equation 32 implies that all the 'phase space' coordinates x_i and p_i are independent of s, in which case:

$$\nabla\left(\frac{1}{2}n^2\right) = \frac{d^2\mathbf{r}}{ds^2} \qquad (33)$$

gives zero on the right-hand side even if the refractive index has a non-zero gradient. However, this interpretation is a bit hasty. All that we have shown so far is that H is numerically equal to zero, that the kinetic and potential 'energies' cancel out. But H is still a function of **r** and **p**. Such a case exists in mechanics. The Hamiltonian for a comet moving about the sun is:

$$H(\mathbf{r},\mathbf{p},\mathbf{J}) = \frac{p^2}{2m} + \frac{J^2}{2mr^2} - G\frac{Mm}{r}\ , \qquad (34)$$

where **p** is the linear momentum and **J** is the angular momentum. One can write Hamilton's equations for this comet, even in the case where the trajectory is parabolic; where the numerical value of the Hamiltonian is zero.

It is in this sense that we interpret the result H = 0. H is a function of the canonical momenta and the generalized coordinates, but the numerical values of the kinetic and potential energies happen to cancel out. This requires that the optical potential energy U be everywhere negative, which Equation 28 shows is the case.

Now, let us find H(**r**,**p**) using the result that n = r'. This 'gauge-fixing' condition turns the canonical momenta of Equation 10 into:

$$p_i = x_i' \qquad (35)$$

and since n = r', Equation 35 yields another numerical relationship:

$$p = (p_i\ p_i)^{\frac{1}{2}} = r' = n\ . \qquad (36)$$

Therefore, the Hamiltonian becomes.

$$H = p_i x_i' - L = p^2 - p\ n(\mathbf{r})\ . \qquad (37)$$

Substituting Equation 36 into Equation 37 shows that H is numerically equal to zero. It is the function on the right-hand side of Equation 37 that we now employ in Hamilton's equations.

From Equation 32, we obtain:

$$\frac{d\mathbf{p}}{ds} = p\ \nabla n\ . \qquad (38)$$

Using the numerical relationship p = n, Equation 38 becomes:

$$\frac{d\mathbf{p}}{ds} = \nabla\left(\frac{1}{2}\ n^2\right). \qquad (39)$$

From Equation 32, it follows that :

$$\frac{dx_i}{ds} = (2p - n)\left(\frac{dp}{dp_i}\right)\ , \qquad (40)$$

yielding:

$$\frac{dx_i}{ds} = (2p - n)\left(\frac{p_i}{p}\right). \qquad (41)$$

Again using the numerical equivalence of p and n, Equation 41 becomes:

$$\frac{d\mathbf{r}}{ds} = \mathbf{p}\ . \qquad (42)$$

Combining the two first-order differential equations (39 and 42) into one second-order equation, we obtain the familiar result:

$$\frac{d^2\mathbf{r}}{ds^2} = \nabla\left(\frac{1}{2}n^2\right). \qquad (43)$$

Thus, Hamilton's equations are consistent with our 'mechanization of geometrical optics'.

Now, to find the Hamilton-Jacobi equation for geometrical optics. In Hamilton-Jacobi theory, one seeks a canonical transformation from the original phase space variables (x_i, p_i) to new phase space variables (X_i,P_i) where the new variables are constants of the motion. To carry out this transformation, one solves the Hamilton-Jacobi equation for the generating function G, which is a function of the independent variable (t in mechanics and s in geometrical optics), the original generalized coordinates, and the new canonical momenta (which are constants of the motion). The original canonical momenta and the new generalized coordinates (which are also constants of the motion) are related to G by:

$$p_i = \frac{\partial G}{\partial x_i} \qquad X_i = \frac{\partial G}{\partial P_i} \; . \tag{44}$$

The Hamilton-Jacobi equation is

$$H\left(s, x_i, \frac{\partial G}{\partial x_i}\right) + \frac{\partial G(s, x_i, P_i)}{\partial s} = 0 \; . \tag{45}$$

Notice that the total derivative of G with respect to s is:

$$\frac{dG}{ds} = \frac{\partial G}{\partial s} + x_i' \left(\frac{\partial G}{\partial x_i}\right) \; . \tag{46}$$

Combining Equation 46 with Equation 44 and the Hamilton-Jacobi equation yields the numerical result:

$$\frac{dG}{ds} = -H + x_i' \, p_i = L \tag{47}$$

thus:

$$G = \int L \, ds \; . \tag{48}$$

Since H = 0, Equation 45 shows that G does not depend explicitly on s:

$$\frac{\partial G}{\partial s} = 0 \; . \tag{49}$$

This means that the functional, $\int L \, ds$, does not depend explicitly on s. This is as it should be because s was put in artificially at the outset. So, the 'mechanization of geometrical optics' is also consistent with the Hamilton-Jacobi equation.

APPLICATIONS OF THE THEORY

Let us examine some examples of the application of the 'mechanization of geometrical optics' algorithm.

A RAY PASSING THROUGH AN INTERFACE BETWEEN 2 DIFFERENT MEDIA

The potential for this system ($-1/2 \, n^2$) is a piecewise constant that is independent of x. The 'optical Newton's second law' predicts that in the x direction:

$$x'' = 0 \tag{50}$$

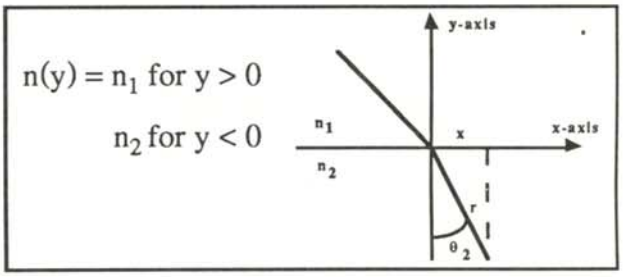

Since dx/ds is constant, dx/ds must be continuous across the plane y = 0. With $x = r \sin\theta$ this condition becomes:

$$\left(\frac{dr}{ds}\right)_1 \sin\theta_1 = \left(\frac{dr}{ds}\right)_2 \sin\theta_2 \; . \tag{51}$$

Using our result that n = r', we recognize Equation 51 as Snell's law:

$$n_1 \sin\theta_1 = n_2 \sin\theta_2 \; . \tag{52}$$

ROAD MIRAGE

Road mirage phenomenology can be modeled by supposing the refracive index increases with height above the road. To the first order in y:

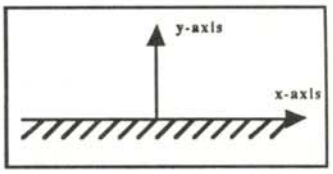

$$n(y) \cong n(0) + y\left(\frac{dn}{dy}\right)_0 = n_o + a\,y \; . \tag{53}$$

Then the 'optical Newton's second law' becomes:

$$x'' = 0 \quad y'' = a\,(n_o + ay) \tag{54}$$

with solutions:

$$x \, \alpha \, s \qquad y \, \alpha \cosh(as) \tag{55}$$

Eliminating s gives:

$$y \, \alpha \cosh(ax) \tag{56}$$

So the ray 'hangs' above the road surface, just as a chain of uniform density hangs in a constant

gravitational field.

CENTRAL FIELD FOR OPTICS

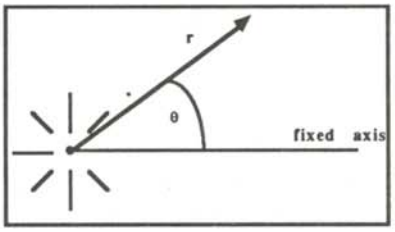

This case arises whenever $n(\mathbf{r}) = n(r)$, where r is some distance from a 'force center'. Then $U(\mathbf{r}) = U(r)$. the problem is formally identical to that of a particle moving in a central field. There will be a conserved 'optical angular momentum':

$$\mathbf{J} = \mathbf{r} \times \mathbf{r}' \tag{57}$$

where:

$$\mathbf{r}' = r\,\hat{r} + r\theta'\,\hat{\theta}\ , \tag{58}$$

so that:

$$J = r^2\,\theta'\ . \tag{59}$$

The total 'optical energy' is conserved and is numerically equal to the Hamiltonian.

$$H = \frac{1}{2}\,r'^2 + U \tag{60}$$

becomes:

$$0 = \frac{1}{2}\,r'^2 + \frac{J^2}{2r^2} - \frac{1}{2}\,n^2\ . \tag{61}$$

This can be solved for:

$$r' = \left(\frac{dr}{d\theta}\right)\theta' \tag{62}$$

and using Equation 59 gives:

$$\theta = \int\left[n^2 - \frac{J}{r^2}\right]^{\frac{1}{2}}\left(\frac{J}{r^2}\right)dr\ . \tag{63}$$

In the special case where:

$$-\frac{1}{2}n^2 = -\frac{k}{r}\ \text{(with } k > 0\text{)}, \tag{64}$$

we already know the answer. The ray's trajectory is a conic section with the focus at the origin. The eccentricity is:

$$e = \left[1 + \frac{2J^2E}{k^2}\right]^{\frac{1}{2}}, \tag{65}$$

but since E = 0, the trajectory is a parabola.

REFERENCES

1 J. Evans and M. Rosenquist, Am. J. Phys, 54, 1986 p. 876-883.

FACULTY SPONSOR

Dr. Dwight E. Neuenschwander
Department of Physics
Southern Nazarene University
Bethany, OK 73008

THE CHAOTIC DYNAMICS OF A BOUNCING BALL

Stephen R. Levengood
Department of Physics
Fort Lewis College
Durango, CO 81301

ABSTRACT

Tufillaro and Albano [1] have described an experiment which illustrates the periodic doubling route to chaos in the nonlinear dissipative system of a bouncing ball driven by a table with sinusoidal motion. Our attempts to repeat the experiment produced results which are not in agreement with their description. In particular, we observed period three orbits at a parameter value inconsistent with the interpretation of the bouncing ball as a one dimensional dynamical system. This implies that the quadratic map is not analogous to the system of the bouncing ball, thus raising doubt about the analysis presented in the previous work.

1. N.B. Tufillaro and A.M. Albano, "Chaotic Dynamics of a Bouncing Ball", Am.Jour. Phys., 54, 10, Oct. 1986, pp. 939-944.

INTRODUCTION

N.B. Tufillaro and A.M. Albano described an experiment, intended to introduce students to the chaotic dynamics of a simple nonlinear dissipative system, which illustrates the period doubling route to chaos [1]. The mechanical system consisted of a bouncing ball driven by a table that had a sinusoidal motion. The angular frequency of the table was held constant and the amplitude of the motion varied. Our attempts to repeat the experiment have raised some difficult questions about the original interpretation. If the reader is not familiar with some of the concepts of chaotic systems and period doubling, an excellent introduction can be found in Hofstadter.[2]

Stephen Levengood graduated from Fort Lewis College in April, 1991. During the summers, he works as a construction inspector for the Colorado Highway Department and enjoys riding his mountain bicycle near his home in Breckenridge, Colorado, a small, high altitude resort twon known for its skiing. He is presently attending graduate school in physics at the University of Oklahoma at Norman, where he has a teaching assistantship..

QUALITATIVE DESCRIPTION OF THE BOUNCING BALL

In the 1986 experiment, the bouncing ball was driven by a table vibrating sinusoidally with an amplitude A and frequency ω as shown in Figure 1. The amplitude of the table was varied for a fixed frequency. When the amplitude was small, the ball and table moved together. However, when the value of A was greater than g/ω^2, where g is the acceleration due to gravity, the ball was thrown off the moving table and be-

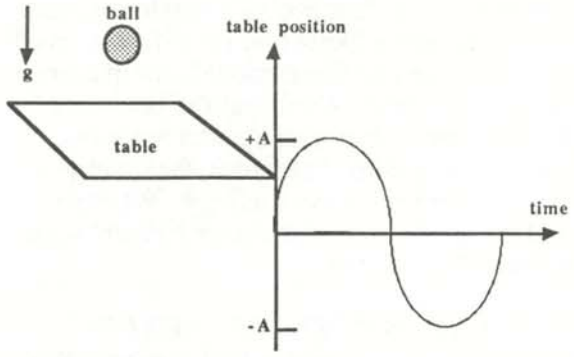

Figure 1
The bouncing ball driven by a sinusoidally vibrating table. [1]

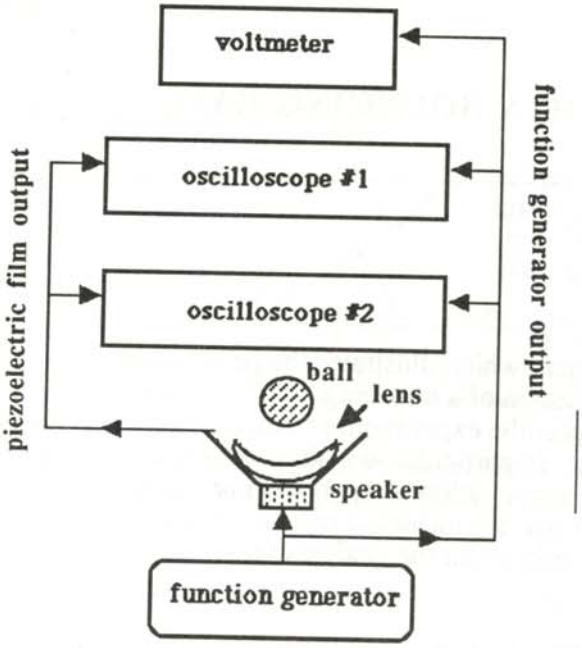

Figure 2
The experimental set-up.

gan to bounce.

The authors interpretation was that at first, the motion of the ball will repeat itself every bounce, hence a period $T = 2\pi/\omega$. At a higher value of A, if the table and ball were truly a one dimensional dynamical system, the period would double to 2T. At even higher values of A, the period would double yet again to 4T, to 8 T and so on. Finally, at a critical value of A, the system would exhibit chaos. The values of the amplitude at which the doubling would occur could be determined by Feigenbaum's Delta. [1] The iteration of a function of a single real variable, Feigenbaum's Delta and the bifurcations diagram describe one-dimensional, one-parameter systems. However, we found the bouncing ball is neither a one-parameter system nor a one-dimensional system. Therefore, the quadratic map is not an instructive analogy. We also found it not possible to measure Feigenbaum's Delta with this system.

EXPERIMENTAL SETUP

The setup for our bouncing ball experiment is shown in Figure 2. A speaker, driven by a sinusoidal function generator, was used as the vibrating table. The ball bounced on a concave lens attached to the speaker. Fastened to the top of the lens with a piece of double edged clear tape was a piece of piezoelectric film 28 μm thick. The piezoelectric film generated a small voltage every time the ball impacted upon it.

Two oscilloscopes monitored the outputs of both the piezoelectric film and the function generator. The first showed a series of spikes on one channel as the ball impacted the film and displayed the sinusoidal voltage sent to the

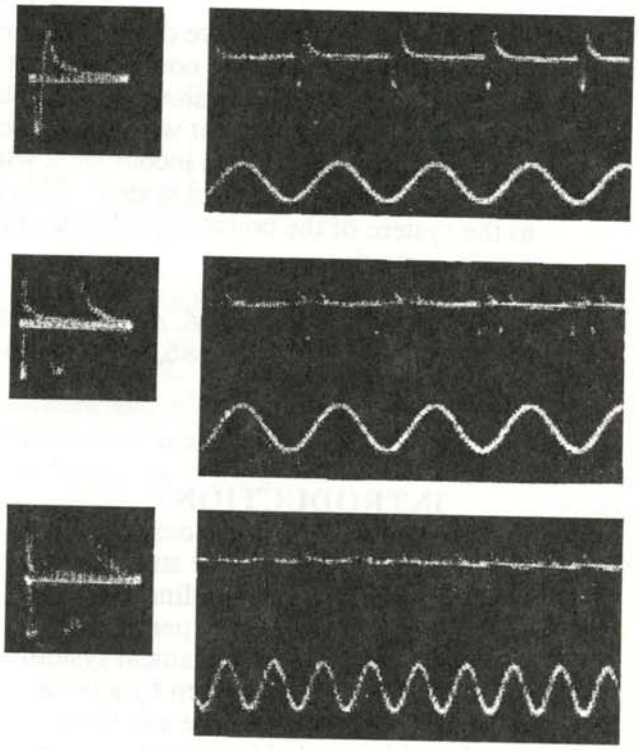

Figure 3

Top left: The X-Y pattern with the output of the piezoelectric film plotted on the Y-axis and the output from the function generator plotted on the X-axis. It is the one downward spike that is of interest and which shows this to be a period one orbit.

Top right: The dual trace of the output from the piezoelectric film (upper) and the output of the function generator (lower). Once again, we are interested in the downward spike. The motion repeats every bounce, therefore, it is a period one orbit.

Middle left: The downward spikes signify that this is an orbit of period two.

Middle right: The dual trace shows that the motion repeats every two bounces, therefore, it is a period two orbit.

Bottom left: Four downward spikes signify that this is an orbit of period four.

Bottom right: The motion is repeated every four bounces, so this is an orbit of period four.

speaker on the other. The second oscilloscope displayed the output from the piezoelectric film on the y-axis and the output from the function generator on the x-axis. The Lissajous style pattern let us more closely observe the phase difference between the two inputs than is possible with just the first oscilloscope.

The experimental set up used by Tuffilaro et. al. was similar, except for the use of the X-Y pattern. We also used both a steel ball (0.18 g) and glass balls of different sizes.

RESULTS

WITH THE SMALL STEEL BALL

A typical data collection sequence is as follows. At a frequency of about 80 Hz, the voltage to the speaker was slowly increased. At 2.08V, the motion of period one began. When the voltage was increased slowly to 2.17V, a splitting in the X-Y pattern was observed: the motion of period two was first seen. At 2.23 V, another doubling was observed: period four. As the voltage was further increased, chaotic motion was observed. Periods higher than four were not seen.

When this procedure was repeated at a more rapid rate of increase of the voltage applied to the speaker, we found periods of one, two and four at voltages of 1.80V, 1.85V, and 1.88V respectively. Similar results were seen at other frequencies. Figure 3 shows both the X-Y and dual trace pictures for periods of one, two, and four at 100 Hz. Figure 4 is a pictorial representation of the motion of the ball and the lens.

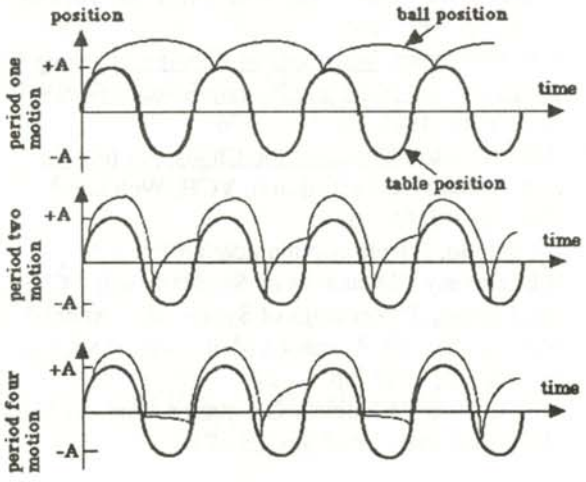

Figure 4

A pictorial representatin of period one, two and four motion. Notice that the height the ball bounces is determined (at least in part) by when the ball impacts the table.

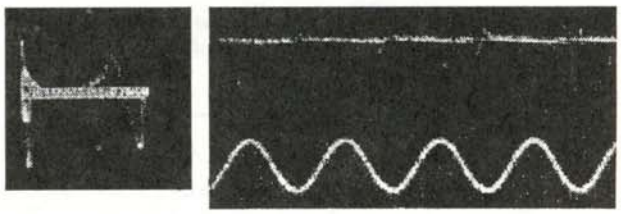

Figure 5

Left: The Lissajous style pattern shows three downward (on the left side of the trace we see one smaller spike on top of a larger spike) which means one bounce impacted the piezoelectric film harder than the other. These two bounces impact at different times because the Lissajous style pattern is sinusoidal on the X-axis, therefore, it moves slower at the ends. One bounce impacts when the trace is moving one direction and the other impacts when the trace is moving in the other direction, so they do not impact the table at the same place.

Right: Dual trace for the orbit of period three. The motion repeats itself every three bounces.

Figure 3 shows periods of one, two and four instead of periods of T, 2T and 4T. This suggests that the motion of the table was emphasized in the previous experiment more than was necessary.

If Feigenbaum's Delta did apply to our data, the period four motion should begin about 2.19V in the first case and at 1.86V in the second case. Our data did not seem to agree with Feigenbaum's Delta.

When the voltage applied to the speaker was decreased, some interesting results occurred. Instead of finding a period 'halving, the data displayed a hysteresis. At a frequency of about 90 Hz, where it was difficult to even observe a steady doubling, a fairly stable period of three was observed at a voltage below the value where motion of period one was observed.

At a frequency of approximately 100 Hz, a short lived period three motion was observed at a voltage below the value where period four motion first occurred. Since the motion was unstable, it was lost several times, However, after some experimentation, it became possible to bring the period three motion back on demand. The oscil-

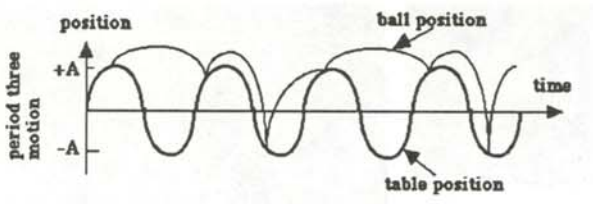

Figure 6
A pictorial representation of period three motion.

loscope patterns are shown in Figure 5. Figure 6 is a pictorial representation of the motion.

The implications of finding motion of period three are important. The observation of period three motion at an amplitude less than the amplitude where motion of period one first occurs implies that the conditions under which Sarkovskii's Theorem holds are not present in the system of the bouncing ball. [3] The bouncing ball system is analogous to the case of a simple pendulum subject to torque and friction. This system is multi-dimensional instead of one-dimensional. Therefore, the theoretical results for a system consisting of the iteration of a function of a single real variable do not apply to this system. Likewise, it follows that the conditions of Sarkovskii's Theorem do not apply either. [4-6]

GLASS BALLS

When a glass ball of mass 0.0829 g was placed in the apparatus operating at 80 Hz, motion of period one began at 1.06V. At higher voltages, we found chaotic motion instead of periodic motion. For the larger glass ball of mass 0.2708 g, the period one motion was first observed at 1.20V. Since the mass of the larger glass ball was larger than that of the steel ball-bearing, these results indicate behavior that is dependent upon the coefficient of restitution, which is dependent upon the type of material used, and not the mass.

As the balls were bouncing upon the easily deformed piezoelectric film, the coefficients of restitution were rather small. Bouncing the balls on the stationary lens gave values of 0.3 and 0.4 for the glass and steel balls respectively. These low values would definitely have a significant damping effect on the motion of the ball. This is further evidence that the system is not a one parameter system.

Another factor that may contribute to the motion of the steel ball-bearing and not the glass balls is the interaction with the magnet in the speaker. Since the steel ball is of relatively low mass, its motion could be somewhat perturbed by the magnet field. Even a small perturbation could affect an accumulating system of this nature enormously.

A more general implication of this experiment might be that the universe is a much more complex place that it might at first appear, even in the case of a seemingly simple system as that of a bouncing ball. One needs only to dig a little deeper to see that complexity.

ACKNOWLEDGEMENTS

The author would like to thank Gene Folsom and Dr. Jerry Crawford for the time and effort needed to produce the CCD pictures of the oscilloscope traces. He also thanks Dr. Crawford for his help in setting up the experiment and for the idea to use the Lissajous style pattern to observe the motion of the ball. He also would like to thank Dr. Tom Norton for the suggestion to use glass balls to test whether the coefficient of restitution had an effect upon the motion of the ball. Finally, he would like to extend his gratitude to Dr. James Costello for his time, effort and patience.

REFERENCES

1. N.B. Tufillaro and A.M. Albano, "Chaotic Dynamics of a Bouncing Ball"' Am. Jour. Phys. 54, 10, Oct. 1986, pp. 939 - 944.
2. D.R. Hofstatder, Metamagical Themas: Questing for the Essence of Mind and Pattern, Bantam Books, Inc., New York, 1985, pp. 364 - 376.
3. H.G. Schuster, Deterministic Chaos, An Introduction, Second Revised edition, VCH, Weinheim, 1986, pp 40, 65 - 67.
4. J. Costello, private communication.
5. R.L. Devany, "Dynamics of Simple Maps, " Chaos and Fractals, Proceedings of Symposia in Applied Mathematics, 39, Advanced Mathematical Society, Providence, 1989, pp. 1 - 24.
6. P.H. Holmes, "Nonlinear Oscillations and the Smale Horseshoe Map", Ibid, pp. 25 - 27.

FACULTY SPONSOR

Dr. James Castello
Department of Physics
Fort Lewis College
Durango, CO 81301

The Journal of Undergraduate Research in Physics

The **Journal of Undergraduate Research in Physics** is the journal of Sigma Pi Sigma and the Society of Physics Students. It is published by the Physics Department of Guilford College, Greensboro NC. Inquiries about the journal should be sent to the editorial office.

Editorial Office -

Physics Department
Guilford College
Greensboro, NC 27410
919-316-2279 (voice)
919-316-2951 (FAX)

Editor -

Dr. Rexford E. Adelberger
Professor of Physics
Department of Physics
Guilford College
Greensboro, NC 27410

Editorial Board -

Dr.Raymond Askew
Space Power Insitute
Auburn University

Dr. László Baksay
Department of Physics & Astronomy
The University of Alabama

Dr. Sheridan Simon
Department of Physics
Guilford College

The Society of Physics Students

National Office -

Dr. Donald Kirwin, Executive Director
Dr. Edwin Goldin, Associate Director
Society of Physics Students
American Institute of Physics
1825 Connecticut Avenue, N.W.
Suite 213
Washington, DC 20009
202-232-6688

President of the Soceity -

Dr. Jean Krisch
Department of Physics
University of Michigan

President of Sigma Pi Sigma -

Dr Reuben James
Department of Physics
SUNY College at Oneonta